

Article

A Volume Averaging Theory for Convective Flow in a Nanofluid Saturated Metal Foam

Wenhao Zhang ¹, Wenhao Li ¹, Chen Yang ² and Akira Nakayama ^{1,3,*}

¹ Department of Mechanical Engineering, Shizuoka University, 3-5-1 Johoku, Naka-Ku, Hamamatsu 432-8561, Japan; zhangsullivan@gmail.com (W.Z.); powerliwh@163.com (W.L.)

² School of Chemical Engineering, Fuzhou University, Fuzhou 350116, China; yc_hust@126.com

³ School of Civil Engineering and Architecture, Wuhan Polytechnic University, Wuhan 430023, China

* Correspondence: nakayama.akira@shizuoka.ac.jp; Tel.: +81-53-478-1049

Academic Editors: Mehrdad Massoudi and Phuoc X. Tran

Received: 6 January 2016; Accepted: 29 February 2016; Published: 8 March 2016

Abstract: A rigorous derivation of the macroscopic governing equations for convective flow in a nanofluid saturated metal foam has been conducted using the volume averaging theory originally developed for analyzing heat and fluid flow in porous media. The nanoparticle conservation equation at a pore scale based on the Buongiorno model has been integrated over a local control volume together with the equations of continuity, Navier–Stokes and energy conservation. The unknown terms resulting from the volume averaging procedure were modeled mathematically to obtain a closed set of volume averaged versions of the governing equations. This set of the volume averaged governing equations was analytically solved to find the velocity, temperature and nanoparticle distributions and heat transfer characteristics resulting from both thermal and nanoparticle mechanical dispersions in a nanofluid saturated metal foam. Eventually, the analysis revealed that an unconventionally high level of the heat transfer rate (about 80 times as high as the case of base fluid convection without a metal foam) can be attained by combination of metal foam and nanofluid.

Keywords: metal foam; nanofluid; thermal non-equilibrium; dispersion; conductivity

1. Introduction

Recent advances of manufacturing technologies have made metal foams commercially available [1–3]. Naturally, they acquire high specific surface, high thermal conductivity and comparatively high permeability. Thus, metal foams are great candidates for efficient heat exchangers because they possess high interstitial heat transfer between the metal and passing fluid, while a pressure drop is only moderate due to a high permeability.

On the other hand, nanofluids, namely, fluids containing thermally conducting submicron solid particles, are known to have great potential as a high-energy carrier. Larger-sized particles cause numerous problems such as abrasion, clogging and high pressure loss, whereas these nanoparticles such as titania, alumina and copper oxide can stably be suspended within the fluids without causing settling out of suspension. A number of investigations on nanofluids were carried out for the past decade, in order to study their great potential as a high-energy carrier as well as their promising feature of high effective thermal conductivity (e.g., [4–10]). Thus, combination of metal foams and nanofluids, namely, nanofluid saturated metal foams may bring us to a new generation of high performance heat exchangers.

A set of volume averaged transport equations appropriate for convection in nanofluid saturated metal foams was obtained by Sakai *et al.* [11], on the assumption that local thermal equilibrium holds between fluid and metal phases, in which the volume averaged fluid temperature is assumed equal to

that of metal temperature. In reality, the local thermal equilibrium assumption may fail, because the thermal conductivity of metal conducting heat from the wall is much higher than that of nanofluid.

Kuwahara *et al.* [12] carried out an elegant analysis to obtain a set of exact solutions for the case of forced convection in a channel filled with a fluid saturated metal foam. They demonstrated that forced convection in a channel subject to constant wall heat flux must be treated using a thermal non-equilibrium model, for the fluid and solid phases within the channel are never at thermal equilibrium. Yang *et al.* [13] faithfully followed their work, and compared the set of exact solutions based on local thermal equilibrium against that based on local thermal non-equilibrium models for the case of tube flows. Eventually, they concluded that substantial errors result from the assumption of local thermal equilibrium for the case of constant heat flux.

These theoretical investigations reveal that the local thermal equilibrium assumption is not valid within in a metal foam and a local thermal non-equilibrium model must be introduced with an interstitial heat transfer model between nanofluid and metal phases.

Yang and Nakayama [14] and Yang *et al.* [15] pointed out another important feature associated with mechanical mixing within the metal foam, namely, dispersion. The mechanical mixing in heat transfer resulting from porous matrices is termed as thermal dispersion, whereas, in this study, mechanical dispersion in nanoparticles transport is referred to as “nanoparticle mechanical dispersion”, *i.e.*, macroscopic dispersion resulting from porous matrices (It should not be confused with “nanoparticle dispersion” meaning particles dispersed in the base fluid, *i.e.*, microscopic dispersion).

In what follows, an appropriate set of volume averaged transport equations for convection in nanofluid saturated metal foams is derived, exploiting a volume averaging theory [16], and allowing that nanofluid temperature and metal temperature differ from each other, *i.e.*, local thermal non-equilibrium model. Microscopic transport equations, which are based on the Buongiorno model [17] for convective heat transfer in nanofluids, are modified so as to account for the effects of nanoparticle volume fraction distributions on the conservation equations of continuity, momentum and energy. Subsequently, they are integrated within a local averaging volume, to obtain an appropriate set of governing equations in terms of volume averaged dependent variables [18–21]. The various terms associated with interfacial surface integrals [22] and spatial correlations of spatial deviations are subsequently modeled mathematically using the volume averaged dependent variables.

A microscopic analysis (*i.e.*, pore scale analysis) will also be conducted in order to investigate possible functional forms for describing longitudinal and transverse and thermal dispersion components in a nanofluid saturated metal foam. Furthermore, nanoparticle mechanical dispersion (*i.e.*, macroscopic dispersion resulting from porous matrices) will be treated microscopically for the first time, and will be modeled mathematically, considering a pore scale conduit. The analysis reveals that the longitudinal particle mechanical dispersion works either to suppress or to enhance effective diffusion. It depends on the sign of the local phase temperature difference. The transverse counterpart, on the other hand, turns out to be insignificant and therefore can be neglected. Moreover, heat transfer performance evaluation under equal pumping power has been made for the case of forced convective heat transfer in a nanofluid saturated metal foam. The present study reveals that an unconventionally high level of the heat transfer rate (about 80 times more than the case of base fluid convection without a metal foam) is possible by combining metal foam with nanofluid.

2. Modified Buongiorno Equations for Nanofluids

Buongiorno [17] carried out a magnitude analysis on the transport equations, assuming dilute mixture, incompressible flow, no chemical reactions, negligible viscous dissipation, negligible external forces, negligible radiative heat transfer, and local thermal equilibrium between nanoparticles and base fluid. Obviously, local thermal equilibrium holds between the nanoparticles and the base fluid, because the size of nanoparticles is so small that nanoparticle temperature changes in an instant to be at thermal equilibrium with that of surrounding base fluid. As demonstrated by Yang *et al.* [23], the

two-component mixture model proposed by Buongiorno may be modified to account for nanofluid density variation in mass, momentum and energy conservations as

$$\frac{\partial \rho}{\partial t} + \frac{\partial \rho u_j}{\partial x_j} = 0 \tag{1}$$

$$\frac{\partial \rho u_i}{\partial t} + \frac{\partial \rho u_j u_i}{\partial x_j} = -\frac{\partial p}{\partial x_i} + \frac{\partial}{\partial x_j} \mu \left(\frac{\partial u_i}{\partial x_j} + \frac{\partial u_j}{\partial x_i} \right) \tag{2}$$

$$c \left(\frac{\partial \rho T}{\partial t} + \frac{\partial \rho u_j T}{\partial x_j} \right) = \frac{\partial}{\partial x_j} \left(k \frac{\partial T}{\partial x_j} \right) \tag{3}$$

$$\rho_p \left(\frac{\partial \phi}{\partial t} + \frac{\partial u_j \phi}{\partial x_j} \right) = \frac{\partial}{\partial x_j} \left(\rho_p D_B \frac{\partial \phi}{\partial x_j} + \frac{\rho_p D_T}{T} \frac{\partial T}{\partial x_j} \right) \tag{4}$$

where ρ , c , μ and k are the density, heat capacity, viscosity and thermal conductivity of nanofluid, respectively, which depend on the nanoparticle volume fraction ϕ as,

$$\rho = \phi \rho_p + (1 - \phi) \rho_{bf} \tag{5a}$$

$$c = \left(\phi \rho_p c_p + (1 - \phi) \rho_{bf} c_{bf} \right) / \rho \tag{5b}$$

$$\mu = \mu_{bf} \left(1 + a_\mu \phi + b_\mu \phi^2 \right) = \mu_{bf} \left(1 + 7.3\phi + 123\phi^2 \right) \tag{5c}$$

$$k = k_{bf} \left(1 + a_k \phi + b_k \phi^2 \right) = k_{bf} \left(1 + 2.72\phi + 4.97\phi^2 \right) \tag{5d}$$

Brownian and thermophoretic diffusion coefficients are given by

$$D_B = \frac{k_{BO} T}{3\pi \mu_{bf} d_p} \tag{6a}$$

and

$$D_T = 0.26 \frac{k_{bf}}{2k_{bf} + k_p} \frac{\mu_{bf}}{\rho_{bf}} \phi \tag{6b}$$

respectively. Nanofluid thermophysical properties such as μ and k are considered as given functions of ϕ . Equation (5c,d) proposed by Maiga *et al.* [24] are believed to be the most reliable correlations, where the subscripts, p and bf refer to as nanoparticle and base fluid, respectively. Moreover, k_{BO} is the Boltzmann constant and d_p is the nanoparticle diameter. d_p can be anywhere of the order of 1 nm to 100 nm. Li and Nakayama [25] investigated the effect of temperature-dependent thermophysical properties on convective heat transfer rates, and found that variations of base fluid properties due to temperature variation are small enough to be neglected as compared with those effects of nanoparticle volume fraction and temperature. Aladag *et al.* [26] pointed out that nanofluids with high particle volume fraction or within the range of low temperature may deviate from Newtonian characteristics. Therefore, we shall not consider the nanofluids of very high volume fraction or of very low temperature. Detailed discussions on these effects on the thermophysical properties may be found in Corcione [27].

A number of investigators, including Bianco *et al.* [28], concluded that the two-component mixture model is quite capable of describing the nanofluid heat transfer, supporting the Buongiorno magnitudes analysis [17]. It is interesting to note that the energy Equation (3) is identical to that of a pure fluid, except that all properties are functions of ϕ . Naturally, nanoparticle conservation Equation (4) must be solved simultaneously with Equations (1) to (3) for the other dependent variables, since thermophysical properties strongly depend on spatial distribution of ϕ . In some previous analyses, the spatial variations of thermophysical properties including Brownian and thermophoretic diffusion coefficients are neglected for simplicity. As discussed in Yang *et al.* [23], however, such analytical treatments result in substantial errors. Thus, in this study, all these variations will be considered.

Some investigators proposed dynamical models accounting for the effect of nanoparticle random motion on the effective thermal conductivity. However, as pointed out by Kleinstreuer and Feng [29], such explicit modifications on the thermal conductivity are still being debated. This study is unique in the sense that the spatial distribution of the nanoparticle volume fraction is determined by solving the nanoparticle transport equation, and substituted into the empirical formulas as functions of nanoparticle volume fraction to evaluate the local values of the thermal properties.

3. Clear Nanofluid Convective Flow in a Circular Tube

Before treating the cases of nanofluid saturated metal foam, we shall consider the fundamental case of clear nanofluid convective flow (*i.e.*, without a metal foam), namely, hydrodynamically and thermally fully developed flow in a tube subject to constant heat flux. The problem may be described mathematically by writing the governing equations in the cylindrical coordinates (x, r) shown in Figure 1 as

$$\frac{1}{r} \frac{d}{dr} \left(r\mu \frac{du}{dr} \right) - \frac{dp}{dx} = 0 \tag{7}$$

$$\rho c u \frac{\partial T}{\partial x} = \frac{1}{r} \frac{\partial}{\partial r} \left(r k \frac{\partial T}{\partial r} \right) \tag{8}$$

$$\frac{1}{r} \frac{d}{dr} \left(D_B \frac{d\phi}{dr} + \frac{D_T}{T} \frac{dT}{dr} \right) = 0 \tag{9}$$

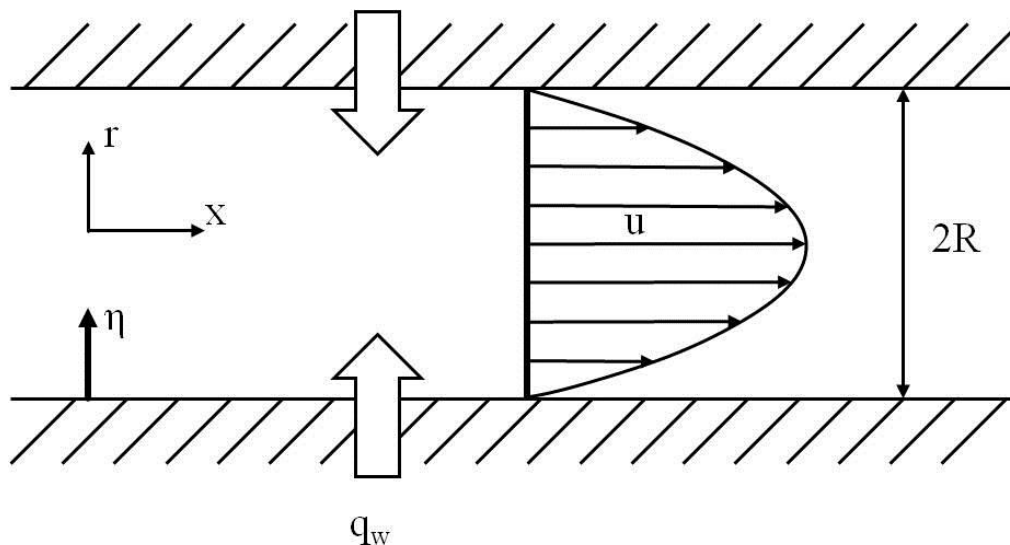


Figure 1. Clear nanofluid convective flow in a tube: hydrodynamically and thermally fully developed flow in a tube subject to constant heat flux.

Yang *et al.* [23] transformed the preceding equations into the set of ordinary differential equations. This set of ordinary differential equations were integrated by using a versatile software SOLODE based on the Runge–Kutta–Gill method [21]. The effects of the bulk mean particle volume fraction ϕ_B on the velocity profile u/u_B are shown in Figure 2a for the case of titania–water nanofluids in a tube with $N_{BT} \equiv D_{Bw} T_w \phi_w k_w / D_{Tw} q_w R = 0.2$ and $\gamma \equiv q_w R / k_w T_w = 0$. Likewise, the temperature profiles are presented in Figure 2b in terms of $(T_w - T) / (T_w - T_B)$. Furthermore, the distributions of the particle volume fraction ϕ/ϕ_B are shown in Figure 2c. The figure indicates low volume fraction of particles near the wall and high volume fraction of particles in the core. This uneven distribution of the volume fraction of particles is caused by the thermophoresis, which drives the particles from the high temperature region near the wall to the low temperature region in the core. The unevenness

grows further as the thermophoretic diffusion dominates over the Brownian diffusion. Due to low and high volume fractions of nanoparticles, the viscosity near the wall surface, as given by Equation (5c), is much smaller than that in the core. This results in the increase in the velocity near the wall and the decrease in the velocity in the core, as can be confirmed in Figure 2a. This tendency is amplified as adding more particles. Figure 2b consistently shows that the increase in the dimensionless velocity near the wall leads to a steeper dimensionless temperature gradient as compared with the one with pure fluids ($\phi_B = 0$). The effects of γ on these profiles are found to be almost negligible, as varying γ from 0 to 0.1. Therefore, all calculations have been carried out with $\gamma = 0$.

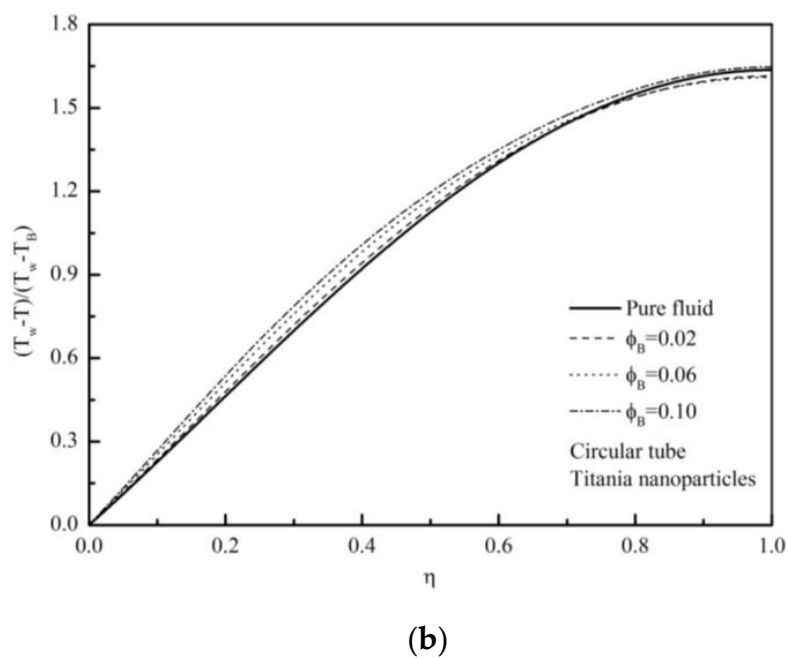
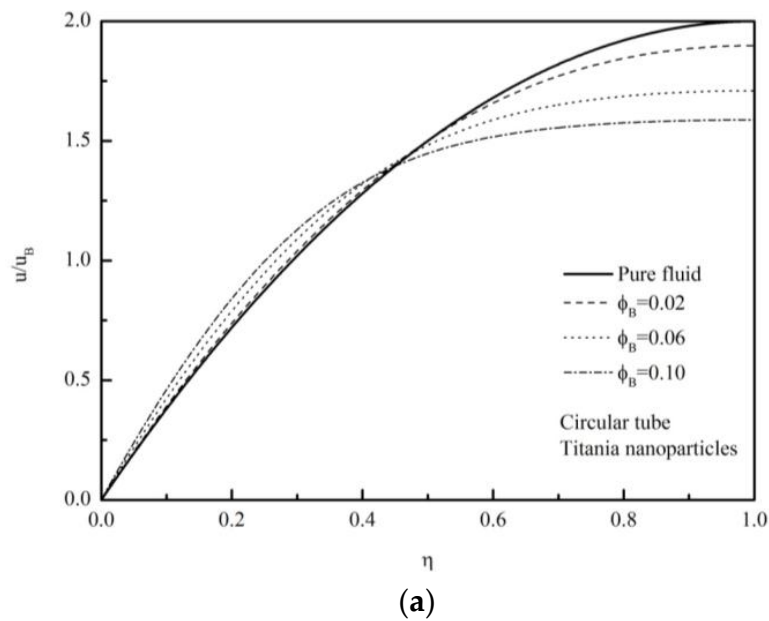


Figure 2. Cont.

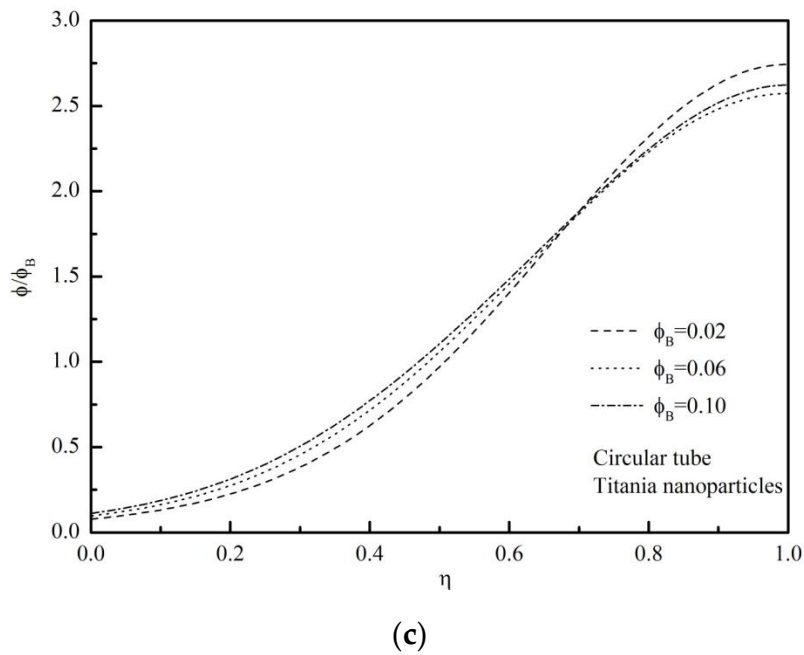


Figure 2. Effects of nanoparticle volume fraction on velocity, temperature and volume fraction profiles in a tube with $N_{BT} = 0.2$ and $\gamma = 0$: (a) velocity profiles; (b) temperature profiles; and (c) volume fraction profiles.

The Nusselt number based on the diameter $D_h = 2R$ and the nanofluid bulk thermal conductivity $k_B = k(\phi_B)$ is given by

$$Nu_B \equiv \frac{hD_h}{k_B} = \left(\frac{hD_h}{k_w} \right) \left(\frac{k_w}{k_B} \right) \tag{10}$$

The Nusselt number Nu_B is expressed in terms of the product of the Nusselt number based on the thermal conductivity at the wall hD_h/k_w and the thermal conductivity ratio k_w/k_B . This thermal conductivity ratio k_w/k_B is always less than 1. Hence, the anomalous heat transfer enhancement, in which the heat transfer coefficient exceeds the level expected from the increase in the effective thermal properties of nanofluids, is possible only when the Nusselt number hD_h/k_w is high enough to make its product (*i.e.*, Nu_B) more than that of pure fluid, namely, 4.36.

Nu_B for the case of alumina nanoparticles is shown in Figure 3, which the anomalous heat transfer enhancement can be seen clearly. Such heat transfer anomaly is absent for the case of channel flow. This difference observed in the heat transfer characteristic may be attributed to the geometrical (radial) effects, namely, that events taking place near the peripheral walls, such as velocity and temperature changes, reflect on bulk quantities more in a tube than in a channel. The maximum value of Nu_B is achieved at $N_{BT} \cong 0.5$ as shown in Figure 3. Figure 4 clearly shows that the degree of the anomalous heat transfer enhancement in titania–water nanofluids is higher than in alumina–water nanofluids. However, as in Figure 5, the heat transfer coefficient of the alumina–water nanofluids is much higher than that of the titania–water nanofluids. This is simply due to the difference in k_B .

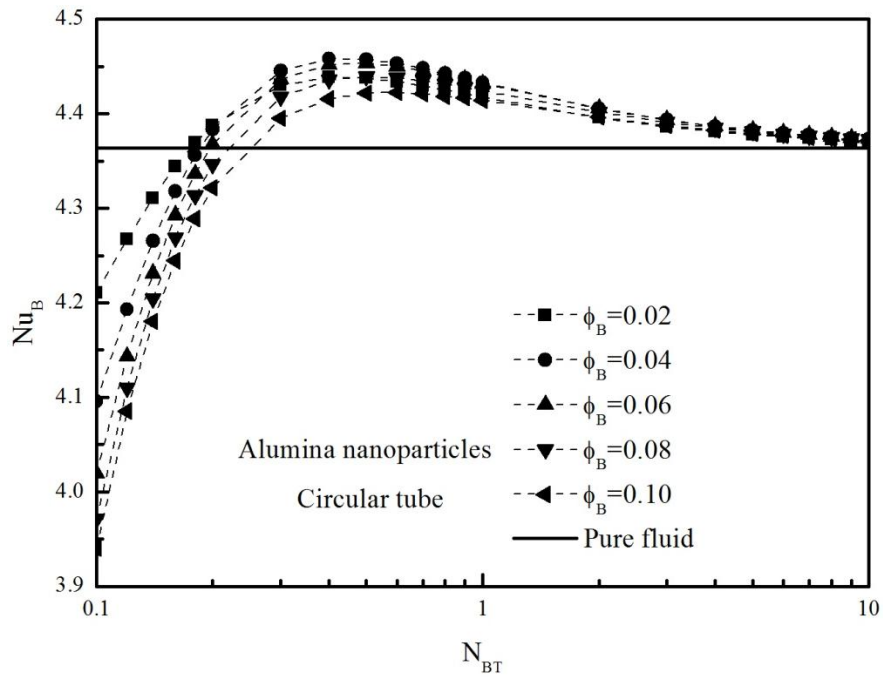


Figure 3. Heat transfer characteristics in alumina–water nanofluids in a tube, Nu_B .

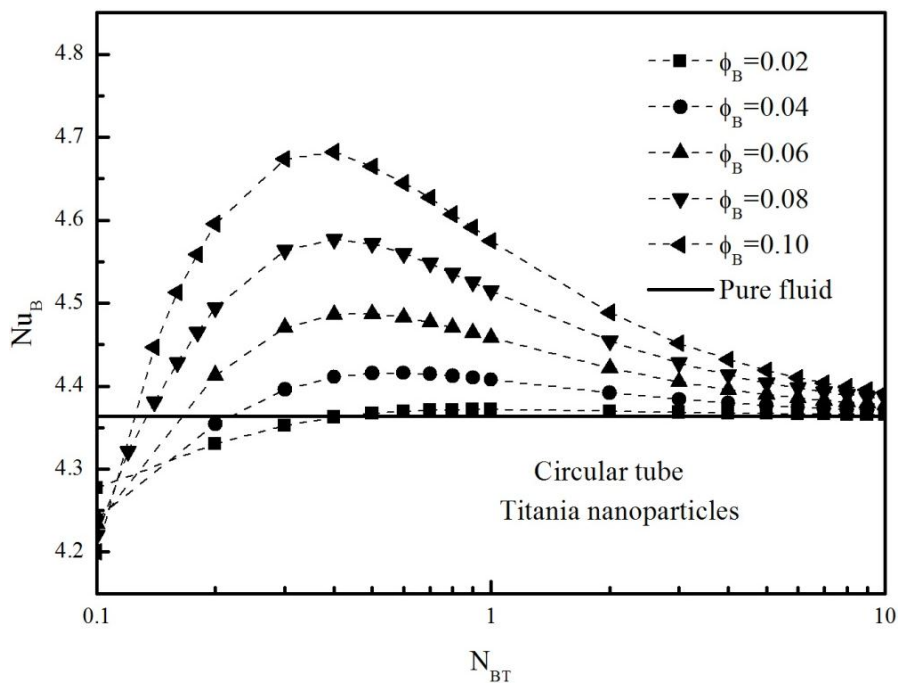


Figure 4. Heat transfer characteristics in titania–water nanofluids in a tube, Nu_B .

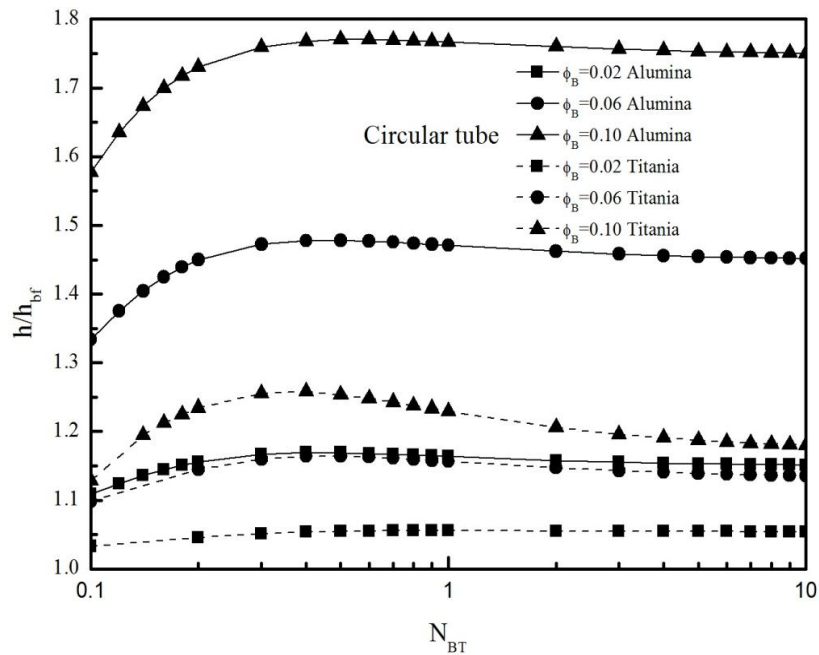


Figure 5. Comparison of the heat transfer coefficients of nanofluids in a tube.

The analysis based on the Buongiorno model equations for convective heat transfer in clear nanofluid flows clearly indicates possible anomalous convective heat transfer enhancement. To be precise, the anomalous heat transfer enhancement has been captured theoretically for various cases of clear nanofluid flows, namely, the cases of titania–water nanofluids in a channel, alumina–water nanofluids in a tube and also titania–water nanofluids in a tube. Comparatively low volume fraction of particles near the wall is responsible for the anomalous heat transfer, because it yields a relatively low viscosity field there, hence, leading to high velocity and steep temperature gradient, near the wall. The maximum Nusselt number based on the bulk mean nanofluid thermal conductivity is observed around at $N_{BT} \cong 0.5$. This finding may be utilized for designing nanoparticles in view of heat transfer enhancement. Moreover, the heat transfer coefficient for the case of alumina–water nanofluids in a tube is seen almost twice higher than that of water in a tube. This substantiates the great potential of nanofluids as a high-energy carrier.

4. Volume Averaging theory

Having confirmed high heat transfer enhancement associated with nanofluids, we shall combine such nanofluids with metal foam, so as to form a passage filled with a nanofluid saturated metal foam. As illustrated in Figure 6a, we expect heat transfer enhancement associated with nanofluids, namely, the anomalous heat transfer resulting from both Brownian diffusion and thermophoretic diffusion, while high effective thermal conductivity and thermal dispersion (*i.e.*, mechanical mixing) can also be expected from an embedded metal foam. These features, when combined together, may bring us the synergy effects on convective heat transfer. Figure 6b clearly indicates that the anomalous heat transfer enhancement in nanofluids, when taking place in a passage filled with a nanofluid saturated metal foam, further leads us to an innovative heat transfer enhancement. The velocity overshooting is expected in the near wall layer, which is partially responsible for the innovative heat transfer enhancement. This interesting feature will be numerically predicted later.

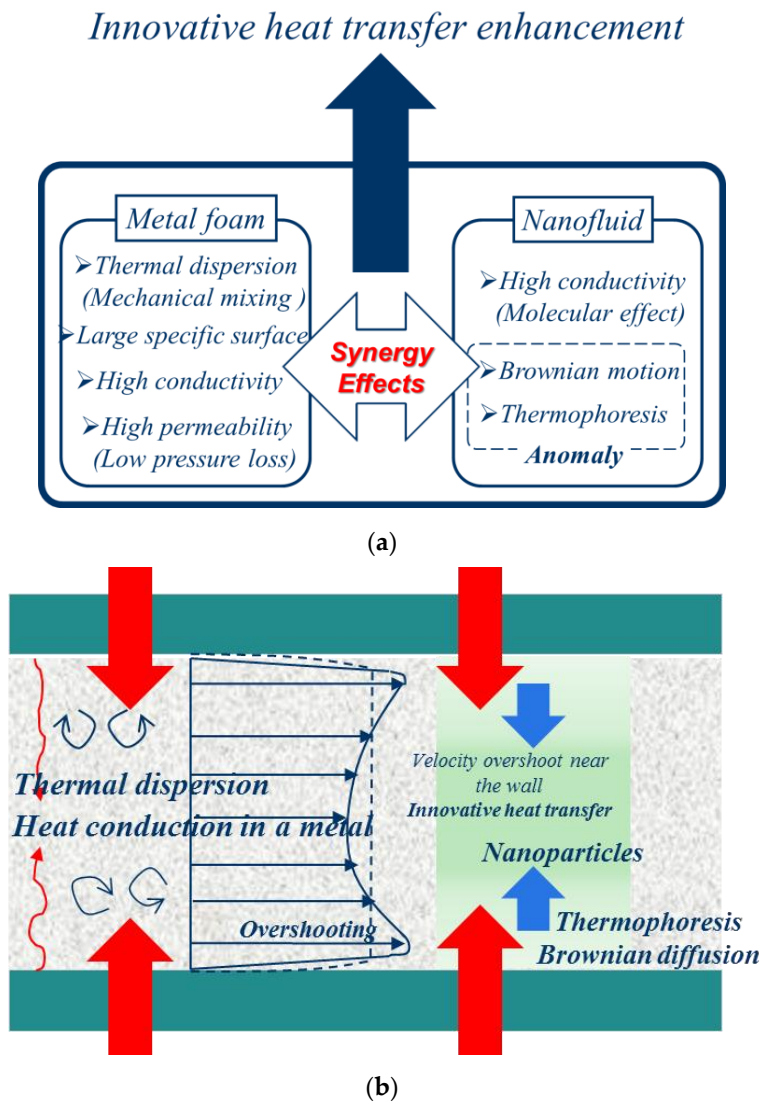


Figure 6. Innovative heat transfer enhancement: (a) synergy effects of nanofluid saturated metal foam on heat transfer; and (b) possible mechanism of heat transfer enhancement.

In order to investigate such an innovative heat transfer enhancement, we shall introduce a volume averaging procedure and seek a complete set of the macroscopic governing equations for convection within a nanofluid saturated metal foam.

Consider a local averaging volume V in nanofluid saturated metal foam, as shown in Figure 7. Its length scale $V^{1/3}$ is much smaller than the macroscopic characteristic length, but, at the same time, much greater than the microscopic characteristic length (see, e.g., [18–21]). This condition allows us to define the volume average of a certain variable φ as

$$\langle \varphi \rangle = \frac{1}{V} \int_{V_f} \varphi dV \tag{11a}$$

Another average, namely, the intrinsic average, is given by

$$\langle \varphi \rangle^f = \frac{1}{V_f} \int_{V_f} \varphi dV \tag{11b}$$

where V_f is a volume space which nanofluid occupies. Obviously, two averages are related as $\langle \varphi \rangle = \varepsilon \langle \varphi \rangle^f$, where $\varepsilon = V_f/V$ is the porosity, namely, local volume fraction of the nanofluid phase. Let us decompose a variable into its intrinsic average and spatial deviation from it:

$$\varphi = \langle \varphi \rangle^f + \tilde{\varphi} \tag{12}$$

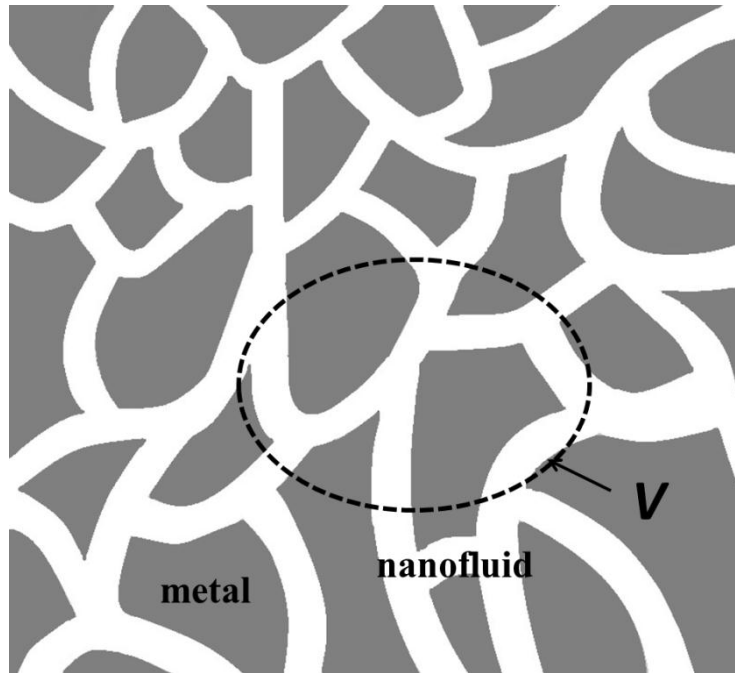


Figure 7. Averaging volume in nanofluid saturated metal foam: averaging volume is smaller than macroscopic characteristic scale but smaller than pore scale.

All dependent variables in the microscopic governing equations for the nanofluid and metal phases are decomposed in this manner. The following spatial average relationships are used:

$$\langle \varphi_1 \varphi_2 \rangle^f = \langle \varphi_1 \rangle^f \langle \varphi_2 \rangle^f + \langle \tilde{\varphi}_1 \tilde{\varphi}_2 \rangle^f \tag{13}$$

$$\left\langle \frac{\partial \varphi}{\partial x_i} \right\rangle = \frac{\partial \langle \varphi \rangle}{\partial x_i} + \frac{1}{V} \int_{A_{\text{int}}} \varphi n_i dA \tag{14a}$$

$$\text{or } \left\langle \frac{\partial \varphi}{\partial x_i} \right\rangle^f = \frac{1}{\varepsilon} \frac{\partial \varepsilon \langle \varphi \rangle^f}{\partial x_i} + \frac{1}{V_f} \int_{A_{\text{int}}} \varphi n_i dA \tag{14b}$$

and

$$\left\langle \frac{\partial \varphi}{\partial t} \right\rangle = \frac{\partial \langle \varphi \rangle}{\partial t} \tag{15}$$

A_{int} represents the interfaces between fluid and solid matrix within a local averaging volume. Note N_i is the unit vector pointing outward from nanofluid side to solid side. All dependent variables for nanofluid and metal phases are decomposed according to Equation (12). Upon exploiting the foregoing spatial average relationships, the microscopic Equations (1) to (4) are integrated over a local averaging volume. The set of macroscopic governing equations thus obtained for nanofluid and metal phases in a nanofluid saturated metal foam with uniform porosity ε may be given as follows:

$$\frac{\partial \rho \langle u_j \rangle^f}{\partial x_j} + \frac{1}{V_f} \int_{A_{\text{int}}} \rho u_j n_j dA = 0 \tag{16}$$

$$\begin{aligned} & \frac{\partial \rho \langle u_i \rangle^f}{\partial t} + \frac{\partial \rho \langle u_j \rangle^f \langle u_i \rangle^f}{\partial x_j} \\ &= -\frac{\partial \langle p \rangle^f}{\partial x_i} + \frac{\partial}{\partial x_j} \left(\mu \left(\frac{\partial \langle u_i \rangle^f}{\partial x_j} + \frac{\partial \langle u_j \rangle^f}{\partial x_i} \right) \right) + \frac{\mu}{V_f} \int_{A_{\text{int}}} (u_i n_j + u_j n_i) dA - \rho \langle \tilde{u}_i \tilde{u}_j \rangle^f + \frac{1}{V_f} \int_{A_{\text{int}}} \left(\mu \left(\frac{\partial u_i}{\partial x_j} + \frac{\partial u_j}{\partial x_i} \right) - p \delta_{ij} \right) n_j dA - \frac{1}{V_f} \int_{A_{\text{int}}} \rho u_j u_i n_j dA \end{aligned} \tag{17}$$

$$\varepsilon c \left(\frac{\partial \rho \langle T \rangle^f}{\partial t} + \frac{\partial \rho \langle u_j \rangle^f \langle T \rangle^f}{\partial x_j} \right) = \frac{\partial}{\partial x_j} \left(\varepsilon k \frac{\partial \langle T \rangle^f}{\partial x_j} + \frac{k}{V} \int_{A_{\text{int}}} T n_j dA - \varepsilon \rho c \langle \tilde{T} \tilde{u}_j \rangle^f \right) + \frac{1}{V} \int_{A_{\text{int}}} k \frac{\partial T}{\partial x_j} n_j dA - \frac{c}{V} \int_{A_{\text{int}}} \rho T u_j n_j dA \quad (18)$$

$$(1 - \varepsilon) c_s \frac{\partial \langle T \rangle^s}{\partial t} = \frac{\partial}{\partial x_j} \left((1 - \varepsilon) k_s \frac{\partial \langle T \rangle^s}{\partial x_j} - \frac{k_s}{V} \int_{A_{\text{int}}} T n_j dA \right) - \frac{1}{V} \int_{A_{\text{int}}} k_s \frac{\partial T}{\partial x_j} n_j dA \quad (19)$$

$$\begin{aligned} & \frac{\partial \langle \phi \rangle^f}{\partial t} + \frac{\partial \langle u_j \rangle^f \langle \phi \rangle^f}{\partial x_j} \\ &= \frac{\partial}{\partial x_j} \left(D_B \frac{\partial \langle \phi \rangle^f}{\partial x_j} + \frac{D_T}{\langle T \rangle^f} \frac{\partial \langle T \rangle^f}{\partial x_j} + \frac{D_B}{V_f} \int_{A_{\text{int}}} \phi n_j dA + \frac{D_T}{V_f \langle T \rangle^f} \int_{A_{\text{int}}} T n_j dA - \langle \tilde{\phi} \tilde{u}_j \rangle^f \right) \\ &+ \frac{1}{V_f} \int_{A_{\text{int}}} \left(D_B \frac{\partial \phi}{\partial x_j} + \frac{D_T}{\langle T \rangle^f} \frac{\partial T}{\partial x_j} \right) n_j dA - \frac{1}{V_f} \int_{A_{\text{int}}} u_j \phi n_j dA \end{aligned} \quad (20)$$

Equation (19) is obtained integrating the conduction equation in a metal phase. In the foregoing equations, many interfacial terms vanish due to no-slip and no-particle flux conditions on the nanofluid–metal interface, namely,

$$u_j = \vec{0} \text{ and} \quad (21a)$$

$$\left(D_B \frac{\partial \phi}{\partial x_j} + \frac{D_T}{T} \frac{\partial T}{\partial x_j} \right) n_j = 0 \quad (21b)$$

As these surface integral terms vanish, the equations reduce to

$$\frac{\partial \rho \langle u_j \rangle^f}{\partial x_j} = 0 \quad (22)$$

$$\frac{\partial \rho \langle u_i \rangle^f}{\partial t} + \frac{\partial \rho \langle u_j \rangle^f \langle u_i \rangle^f}{\partial x_j} = -\frac{\partial \langle p \rangle^f}{\partial x_i} + \frac{\partial}{\partial x_j} \left(\mu \left(\frac{\partial \langle u_i \rangle^f}{\partial x_j} + \frac{\partial \langle u_j \rangle^f}{\partial x_i} \right) - \rho \langle \tilde{u}_i \tilde{u}_j \rangle^f \right) + \frac{1}{V_f} \int_{A_{\text{int}}} \left(\mu \left(\frac{\partial u_i}{\partial x_j} + \frac{\partial u_j}{\partial x_i} \right) - p \delta_{ij} \right) n_j dA \quad (23)$$

$$\varepsilon c \left(\frac{\partial \rho \langle T \rangle^f}{\partial t} + \frac{\partial \rho \langle u_j \rangle^f \langle T \rangle^f}{\partial x_j} \right) = \frac{\partial}{\partial x_j} \left(\varepsilon k \frac{\partial \langle T \rangle^f}{\partial x_j} + \frac{k}{V} \int_{A_{\text{int}}} T n_j dA - \varepsilon \rho c \langle \tilde{T} \tilde{u}_j \rangle^f \right) + \frac{1}{V} \int_{A_{\text{int}}} k \frac{\partial T}{\partial x_j} n_j dA \quad (24)$$

$$(1 - \varepsilon) c_s \frac{\partial \rho \langle T \rangle^s}{\partial t} = \frac{\partial}{\partial x_j} \left((1 - \varepsilon) k_s \frac{\partial \langle T \rangle^s}{\partial x_j} - \frac{k_s}{V} \int_{A_{\text{int}}} T n_j dA \right) - \frac{1}{V} \int_{A_{\text{int}}} k \frac{\partial T}{\partial x_j} n_j dA \quad (25)$$

$$\varepsilon \left(\frac{\partial \langle \phi \rangle^f}{\partial t} + \frac{\partial \langle u_j \rangle^f \langle \phi \rangle^f}{\partial x_j} \right) = \frac{\partial}{\partial x_j} \left(\varepsilon D_B \frac{\partial \langle \phi \rangle^f}{\partial x_j} + \frac{\varepsilon D_T}{\langle T \rangle^f} \frac{\partial \langle T \rangle^f}{\partial x_j} + \frac{D_B}{V} \int_{A_{\text{int}}} \phi n_j dA + \frac{D_T}{V \langle T \rangle^f} \int_{A_{\text{int}}} T n_j dA - \varepsilon \langle \tilde{\phi} \tilde{u}_j \rangle^f \right) \quad (26)$$

In the foregoing equations, the correlations associated with deviations, $-\rho \langle \tilde{u}_i \tilde{u}_j \rangle^f$, $\varepsilon \rho c \langle \tilde{T} \tilde{u}_j \rangle^f$ and $-\varepsilon \langle \tilde{\phi} \tilde{u}_j \rangle^f$, correspond with mechanical dispersion terms, whereas the surface integral terms, $\frac{k}{V} \int_{A_{\text{int}}} T n_j dA$, $\frac{D_B}{V} \int_{A_{\text{int}}} \phi n_j dA$ and $\frac{D_T}{V \langle T \rangle^f} \int_{A_{\text{int}}} T n_j dA$, correspond with the tortuosity terms.

5. Mathematical Modeling

As usual, Forchheimer-extended Darcy law is introduced to describe the internal flow resistance:

$$\frac{1}{V_f} \int_{A_{\text{int}}} \left(\mu \left(\frac{\partial u_i}{\partial x_j} + \frac{\partial u_j}{\partial x_i} \right) - p \delta_{ij} \right) n_j dA \frac{\partial}{\partial x^i} \rho \langle \tilde{u}_i \tilde{u}_j \rangle^f = -\frac{\varepsilon \mu}{K} \langle u_j \rangle^f - \rho \varepsilon^2 b \sqrt{\langle u_k \rangle^f \langle u_k \rangle^f} \langle u_j \rangle^f \quad (27)$$

while tortuosity in nanoparticle volume fraction transport is neglected since

$$\frac{D_B}{V_f} \int_{A_{int}} \phi n_j dA \cong \frac{D_B}{V_f} \phi \int_{A_{int}} n_j dA = \vec{0} \tag{28}$$

Tortuosity terms in two energy equations may be modeled introducing the Yang–Nakayama effective porosity ϵ^* ([12,14]) as

$$\epsilon k \frac{\partial \langle T \rangle^f}{\partial x_j} + \frac{k}{V} \int_{A_{int}} T n_j dA = \epsilon^* k \frac{\partial \langle T \rangle^f}{\partial x_j} \tag{29a}$$

$$(1 - \epsilon) k_s \frac{\partial \langle T \rangle^s}{\partial x_j} - \frac{k_s}{V} \int_{A_{int}} T n_j dA = (1 - \epsilon^*) k_s \frac{\partial \langle T \rangle^s}{\partial x_j} \tag{29b}$$

where the effective porosity may easily be evaluated from

$$\epsilon^* = \frac{k_s - k_{stag}}{k_s - k_f} \tag{30}$$

where k_{stag} is the stagnant thermal conductivity of saturated porous medium, which can readily be measured using a standard method. However, for the cases of high conductivity porous media such as metal foams, satisfying the condition, $k_s/k \gg 3/(1 - \epsilon)$, there is no need to measure the stagnant thermal conductivity of saturated porous medium, since the effective porosity may well be approximated by

$$\epsilon^* = \frac{2 + \epsilon}{3} \tag{31}$$

according to Yang and Nakayama (2010). For example, in the case of aluminum foam and water combination, we typically have $k_s/k \cong 330$ and $\epsilon = 0.90$. Thus, $k_s/k \gg 3/(1 - \epsilon)$ is satisfied such that $\epsilon^* = (2 + 0.9) / 3 = 0.97$. Furthermore, Newton’s cooling law may be adopted for the interstitial heat transfer between nanofluid phase and metal foam as

$$\frac{1}{V} \int_{A_{int}} k \frac{\partial T}{\partial x_j} n_j dA = h_v (\langle T \rangle^s - \langle T \rangle^f) \tag{32}$$

where h_v is the volumetric interstitial heat transfer coefficient. Upon implementing the foregoing mathematical models, the equations reduce to

$$\frac{\partial \rho \langle u_j \rangle}{\partial x_j} = 0 \tag{33}$$

$$\frac{1}{\epsilon} \frac{\partial \rho \langle u_i \rangle}{\partial t} + \frac{1}{\epsilon^2} \frac{\partial \rho \langle u_j \rangle \langle u_i \rangle}{\partial x_j} = - \frac{\partial \langle p \rangle^f}{\partial x_i} + \frac{\partial}{\partial x_j} \left(\frac{\mu}{\epsilon} \frac{\partial \langle u_i \rangle}{\partial x_j} \right) - \frac{\mu}{K} \langle u_i \rangle - \rho b \sqrt{\langle u_k \rangle \langle u_k \rangle} \langle u_i \rangle \tag{34}$$

$$\epsilon c \frac{\partial \rho \langle T \rangle^f}{\partial t} + c \frac{\partial \rho \langle u_j \rangle \langle T \rangle^f}{\partial x_j} = \frac{\partial}{\partial x_j} \left(\epsilon^* k_f \frac{\partial \langle T \rangle^f}{\partial x_j} - \epsilon \rho c \langle \tilde{T} \tilde{u}_j \rangle^f \right) - h_v (\langle T \rangle^f - \langle T \rangle^s) \tag{35}$$

$$(1 - \epsilon) \rho_s c_s \frac{\partial \langle T \rangle^s}{\partial t} = \frac{\partial}{\partial x_j} (1 - \epsilon^*) k_s \frac{\partial \langle T \rangle^s}{\partial x_j} - h_v (\langle T \rangle^s - \langle T \rangle^f) = 0 \tag{36}$$

$$\epsilon \frac{\partial \langle \phi \rangle^f}{\partial t} + \frac{\partial \langle u_j \rangle \langle \phi \rangle^f}{\partial x_j} = \frac{\partial}{\partial x_j} \left(\epsilon D_B \frac{\partial \langle \phi \rangle^f}{\partial x_j} + \frac{\epsilon^* D_T}{\langle T \rangle^f} \frac{\partial \langle T \rangle^f}{\partial x_j} - \epsilon \langle \tilde{\phi} \tilde{u}_j \rangle^f \right) \tag{37}$$

Note that Equation (29a) is exploited to express the particle tortuosity term as

$$\frac{\epsilon D_T}{\langle T \rangle^f} \frac{\partial \langle T \rangle^f}{\partial x_j} + \frac{D_T}{V \langle T \rangle^f} \int_{A_{int}} T n_j dA \cong \frac{\epsilon D_T}{\langle T \rangle^f} \frac{\partial \langle T \rangle^f}{\partial x_j} + (\epsilon^* - \epsilon) \frac{D_T}{\langle T \rangle^f} \frac{\partial \langle T \rangle^f}{\partial x_j} = \frac{\epsilon^* D_T}{\langle T \rangle^f} \frac{\partial \langle T \rangle^f}{\partial x_j} \tag{38}$$

In the foregoing equations, Darcian velocity vector $\langle u_j \rangle = \varepsilon \langle u_j \rangle^f$ is used in place of the intrinsic velocity vector $\langle u_j \rangle^f$.

6. Thermal Dispersion

Our next task in mathematical modelling is to mathematically model mechanical dispersion terms, namely, $-\varepsilon \rho c \langle \tilde{T} \tilde{u} \rangle^f$ and $-\varepsilon \langle \tilde{\phi} \tilde{u} \rangle^f$, in terms of determinable variables. Measurement of mechanical dispersion, however, is quite formidable. Only a limited number of correlations for metal foams are available only for the case of transverse thermal dispersion. Empirical information is not available for longitudinal thermal dispersion in metal foams. As for the nanoparticle mechanical dispersion, neither theoretical nor empirical information exists so far.

Yang and Nakayama [14] claimed that volumetric interstitial heat transfer coefficient is comparatively easy to measure, using a standard method such as the single blow method [30]. Thus, they conducted an analytical consideration in a pore scale, and derived a theoretical relation to estimate thermal dispersion from the volumetric interstitial heat transfer coefficient, as illustrated below.

Along the macroscopic flow direction x , the nanofluid phase energy Equation (35) at steady state may be written as

$$c \rho \langle u \rangle \frac{\partial \langle T \rangle^f}{\partial x} \cong -h_v (\langle T \rangle^f - \langle T \rangle^s) \tag{39}$$

where we have dropped diffusion term, since convection term on the left hand side predominates over axial diffusion term. A magnitude analysis [14] tells us that the diffusive term in Equation (35) is small and may well be neglected for the first approximation. This is usually true when an external scale of the flow system is much larger than a pore scale.

Let us consider a pore scale passage as illustrated in Figure 8. Longitudinal thermal dispersion term may be evaluated using microscopic velocity and temperature profiles prevailing in this pore scale passage as follows:

$$-\varepsilon \rho c \langle \tilde{T} \tilde{u} \rangle^f = -\rho c \langle u \rangle (\langle T \rangle^f - \langle T \rangle^s) \langle (f-1)(g-1) \rangle^f = \frac{(\rho c \langle u \rangle)^2}{h_v} \langle (f-1)(g-1) \rangle^f \frac{\partial \langle T \rangle^f}{\partial x} \tag{40}$$

where the volume averaged temperature difference between two phases has been replaced by the volume averaged temperature gradient, exploiting the preceding macroscopic Equation (39). Hence,

$$-\varepsilon \rho c \langle \tilde{T} \tilde{u} \rangle^f = \varepsilon k_{dis_{xx}} \frac{\partial \langle T \rangle^f}{\partial x} \tag{41}$$

where

$$\varepsilon k_{dis_{xx}} = \frac{(\rho c \langle u \rangle)^2}{h_v} \langle (f-1)(g-1) \rangle^f \tag{42}$$

which is consistent with what is known as gradient diffusion hypothesis [31]. For the volumetric interstitial heat transfer coefficient h_v in Equation (42), the following empirical correlation proposed by Calmidi and Mahajan [3] may be used:

$$Nu_v = \frac{h_v d_m^2}{k_f} = 8.72 (1 - \varepsilon)^{1/4} \left(\frac{1 - e^{-(1-\varepsilon)/0.04}}{\varepsilon} \right)^{1/2} \left(\frac{\langle u \rangle d_m}{\nu} \right)^{1/2} Pr^{0.37} \tag{43}$$

where d_m is the pore diameter. The correlation is based on the one developed by Zhukauskas [32] for cylinders in laminar cross flow. Note that the functions $f(\eta)$ and $g(\eta)$ describe the velocity and temperature profiles, respectively, in a pore passage of diameter d_m as illustrated in Figure 8.

$$u = \langle u \rangle^f f(\eta) \tag{44a}$$

and

$$T - \langle T \rangle^s = (\langle T \rangle^f - \langle T \rangle^s) g(\eta) \tag{44b}$$

where the dimensionless radial coordinate η normal to the pore wall is defined as

$$\eta = 2r/d_m \tag{45}$$

Any reasonable functions may be used for $f(\eta)$ and $g(\eta)$ in Equation (42) to estimate $k_{dis,xx}$ such as laminar fully developed velocity and temperature profiles in a tube with its diameter d_m :

$$f(\eta) = 2(1 - \eta^2) \tag{46a}$$

and

$$g(\eta) = \frac{3}{4}(3 - 4\eta^2 + \eta^4) \tag{46b}$$

Note that $\langle f(\eta) \rangle^f = \int_0^1 2\eta f(\eta) d\eta = 1$ and $\langle g(\eta) \rangle^f = \int_0^1 2\eta g(\eta) d\eta = 1$. Substituting the foregoing profiles into Equation (42) along with Equation. (43), we readily obtain Longitudinal (laminar):

$$\frac{\varepsilon k_{dis,xx}}{k} = \frac{(\rho c \langle u \rangle)^2}{h_v k} \langle (f-1)(g-1) \rangle^f = \frac{3}{8Nu_v} \left(\frac{\rho c \langle u \rangle d_m}{k} \right)^2 = \frac{3}{8} \frac{\left(\frac{\rho c \langle u \rangle d_m}{k} \right)^{3/2} Pr^{0.13}}{8.72(1-\varepsilon)^{1/4} \left(\frac{1 - e^{-(1-\varepsilon)/0.04}}{\varepsilon} \right)^{1/2}} \tag{47}$$

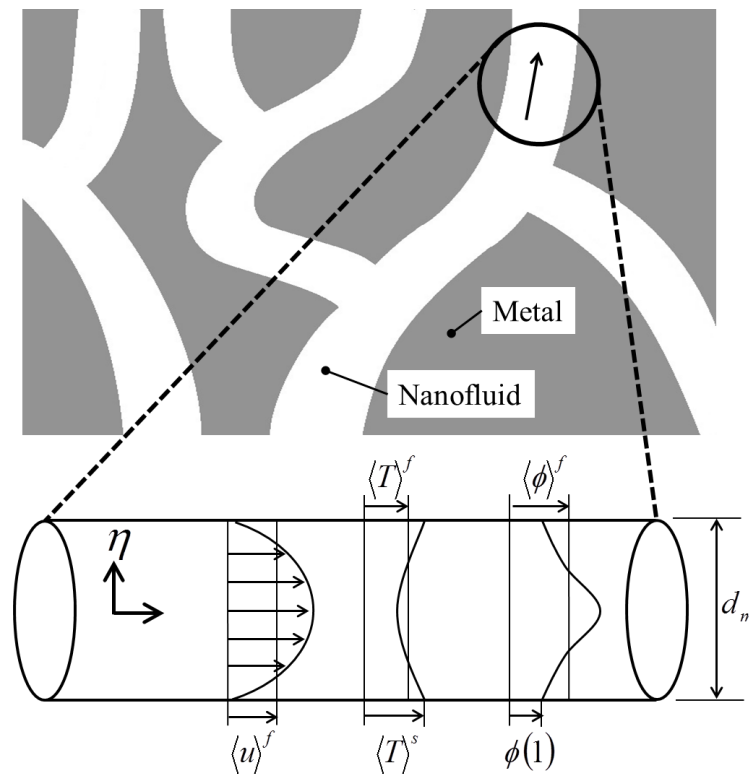


Figure 8. Pore scale passage consideration: pore scale distributions of velocity, temperature and nanoparticles.

A similar relationship can be derived for the transverse thermal dispersion. Let us consider the energy Equation (35) close enough to a heated wall surface for convection to be negligible, but at the

same time, sufficiently away from the wall surface, so that the transverse thermal dispersion dominates over the stagnant thermal diffusion:

$$\varepsilon k_{disyy} \frac{d^2 \langle T \rangle^f}{dr^2} \cong h_v (\langle T \rangle^f - \langle T \rangle^s) \tag{48}$$

which may be integrated to yield

$$\frac{d \langle T \rangle^f}{dr} = -\sqrt{\frac{h_v}{\varepsilon k_{disyy}}} (\langle T \rangle^f - \langle T \rangle^s) \tag{49}$$

such that

$$-\varepsilon \rho c_p \langle \tilde{v} \tilde{T} \rangle^f \equiv \varepsilon k_{disyy} \frac{d \langle T \rangle^f}{dr} = -\rho c_p \langle u \rangle (\langle T \rangle^f - \langle T \rangle^s) \langle F(g-1) \rangle^f = \rho c_p \langle u \rangle \sqrt{\frac{\varepsilon k_{disyy}}{h_v}} \langle F(g-1) \rangle^f \frac{d \langle T \rangle^f}{dr} \tag{50}$$

Hence,

$$\varepsilon k_{disyy} = \frac{(\rho c \langle u \rangle)^2}{h_v} (\langle F(g-1) \rangle^f)^2 \tag{51}$$

where

$$v = \tilde{v} = \langle u \rangle^f F(\eta) \tag{52}$$

such that $\langle F(\eta) \rangle^f = \langle v \rangle^f / \langle u \rangle^f = 0$. Equation (51) obtained for the transverse thermal dispersion conductivity is the same as Equation (42) obtained for the longitudinal thermal dispersion conductivity, except the difference in the multiplicative constants, namely, $(\langle F(g-1) \rangle^f)^2$ and $\langle (f-1)(g-1) \rangle^f$. It is understood that $|F(\eta)| \ll 1$. In fact, the experimental data on packed bed reported by Fried and Combarous [33] suggest that $(\langle F(g-1) \rangle^f)^2$ is much smaller than $\langle (f-1)(g-1) \rangle^f$. In this study, we assume $(\langle F(g-1) \rangle^f)^2 \cong \langle (f-1)(g-1) \rangle^f / 15^2$, such that Transverse (laminar):

$$\begin{aligned} \frac{\varepsilon k_{disyy}}{k} &= \frac{(\rho c \langle u \rangle)^2}{h_v k} (\langle F(g-1) \rangle^f)^2 \\ &= \frac{3}{15^2 \times 8} \frac{\left(\frac{\rho c \langle u \rangle d_m}{k}\right)^{3/2} Pr^{0.13}}{8.72 (1-\varepsilon)^{1/4} \left(\frac{1-e^{-(1-\varepsilon)/0.04}}{\varepsilon}\right)^{1/2}} = 0.00019 \frac{\left(\frac{\rho c \langle u \rangle d_m}{k}\right)^{3/2} Pr^{0.13}}{(1-\varepsilon)^{1/4} \left(\frac{1-e^{-(1-\varepsilon)/0.04}}{\varepsilon}\right)^{1/2}} \end{aligned} \tag{53}$$

In order to estimate the longitudinal thermal dispersion for the case of fully turbulent flow, a similar procedure is used along with the wall laws as

$$u = u_\tau \left(\frac{1}{\kappa} \ln n^+ + B \right) \tag{54a}$$

and

$$T - \langle T \rangle^s = -\frac{q_w \sigma_T}{u_\tau \rho_f c_{pf}} \left(\frac{1}{\kappa} \ln n^+ + A \right) \tag{54b}$$

where u_τ and q_w are friction velocity and wall heat flux, respectively, and $n^+ = u_\tau n / \nu$ is a dimensionless distance measured from the wall surface ($n = (d_m - 2r) / 2$). Moreover, κ is the von-Karman constant while both B and A are empirical constants. It is easy to find

$$\tilde{u} = \frac{u_\tau}{\kappa} \left(\ln \zeta + \frac{3}{2} \right) \tag{55a}$$

and

$$\tilde{T} = -\frac{q_w \sigma_T}{u_\tau \rho c \kappa} \left(\ln \zeta + \frac{3}{2} \right) \tag{55b}$$

where

$$\zeta = 1 - \eta \tag{56}$$

Hence,

$$\begin{aligned} -\varepsilon \rho c \langle \tilde{T} \tilde{u} \rangle^f &= \varepsilon k_{dis_{xx}} \frac{\partial \langle T \rangle^f}{\partial x} = \frac{q_w \sigma_T}{\kappa^2} \left\langle \left(\ln \zeta + \frac{3}{2} \right)^2 \right\rangle^f = \frac{\sigma_T}{\kappa^2} \left\langle \left(\ln \zeta + \frac{3}{2} \right)^2 \right\rangle^f \frac{\rho c \langle u \rangle}{a_f} \frac{d \langle T \rangle^f}{dx} \\ &= \frac{\sigma_T}{4 \varepsilon \kappa^2} \left(\frac{5}{4} \right) \rho c \langle u \rangle d_m \frac{d \langle T \rangle^f}{dx} \end{aligned} \tag{57}$$

where we used Equation (39) to eliminate the wall heat flux $q_w = -\left(h_v/a_f\right) \left(\langle T \rangle^f - \langle T \rangle^s\right)$ with specific surface $a_f = 4\varepsilon/d_m$ in favor of the temperature gradient. Setting κ and σ_T to 0.41 and 0.9, respectively, according to Launder and Spalding [34], we obtain for the turbulent regime.

Longitudinal (turbulent regime):

$$\frac{\varepsilon k_{dis_{xx}}}{k} = \frac{\sigma_T}{4 \varepsilon \kappa^2} \left(\frac{5}{4} \right) \frac{\rho c \langle u \rangle d_m}{k} = \frac{1.67}{\varepsilon} \left(\frac{\rho c \langle u \rangle d_m}{k} \right) \tag{58}$$

Law of the wall was introduced by Taylor [35] to explain high Peclet number dependence observed in dispersion of matter in a pipe flow. The same linear relationship between the thermal dispersion conductivity and Peclet number (as observed experimentally) may easily be deduced using an interstitial heat transfer coefficient correlation, which increases linearly with Peclet number. This linear relationship between the thermal dispersion coefficient and Peclet number was explained theoretically by Nakayama *et al.* [36] for high Peclet number flow through a consolidated porous medium.

As for the transverse dispersion, we again assume $k_{dis_{yy}} \equiv 15^2 k_{dis_{xx}}$, such that Transverse (turbulent regime):

$$\frac{\varepsilon k_{dis_{yy}}}{k} = \frac{\sigma_T}{4 \varepsilon \kappa^2} \left(\frac{5}{4} \right) \frac{\rho c \langle u \rangle d_m}{k} = \frac{1.67}{15^2 \varepsilon} \left(\frac{\rho c \langle u \rangle d_m}{k} \right) = \frac{0.00742}{\varepsilon} \left(\frac{\rho c \langle u \rangle d_m}{k} \right) \tag{59}$$

As for experimental data on metal foams, only those of transverse thermal dispersion are available. The data for transverse dispersion coefficient have been correlated by Calmidi and Mahajan [3] as follows:

Transverse (Calmidi–Mahajan):

$$\frac{\varepsilon k_{dis_{yy}}}{k} = 0.00162 \frac{\left(\frac{\rho c \langle u \rangle d_m}{k} \right)}{\left((1 - \varepsilon)^{0.224} \left(\frac{1.18}{1 - e^{-(1-\varepsilon)/0.04}} \sqrt{\frac{1 - \varepsilon}{3\pi}} \right)^{1.11} \right)^{1/2}} \tag{60}$$

Thus, in Figure 9, Equation (53) for the laminar case and Equation (59) for the turbulent case are plotted together to form a solid curve for the case of $\varepsilon = 0.95$. In the figure, the foregoing empirical correlation Equation (60) is also plotted to examine the validity of the present expressions for the transverse dispersion coefficient. The figure shows fairly good agreement between the solid line based on the present analysis and the dashed empirical line reported by Calmidi and Mahajan. It is noted that Calmidi and Mahajan’s correlation is valid only when the Peclet number $(\rho c \langle u \rangle d_m/k)$ is sufficiently large. Taylor [37] analytically proved that the dispersion coefficient is in proportion to $(\rho c \langle u \rangle d_m/k)^2$, that is consistent with our Equation (47) for the case of small Peclet number, in which the interstitial

heat transfer coefficient stays constant. It is also interesting to note that Gelhar and Axness [38] and Wang and Kitanidis [39] investigated macrodispersion in heterogeneous porous media such as aquifers and geologic formations. They reported Peclet number dependence similar to what is observed in Figure 9. Moreover, Ohsawa [40] in his MS thesis carried out direct numerical simulations for nanofluid forced convection using a numerically generated periodic open-cell. The thermal dispersion numerically predicted by him closely follows the empirical correlation Equation (60) up to Peclet number up to 10,000, or even more. Therefore, the empirical correlation Equation (60) may well be valid in the range as indicated in Figure 9.

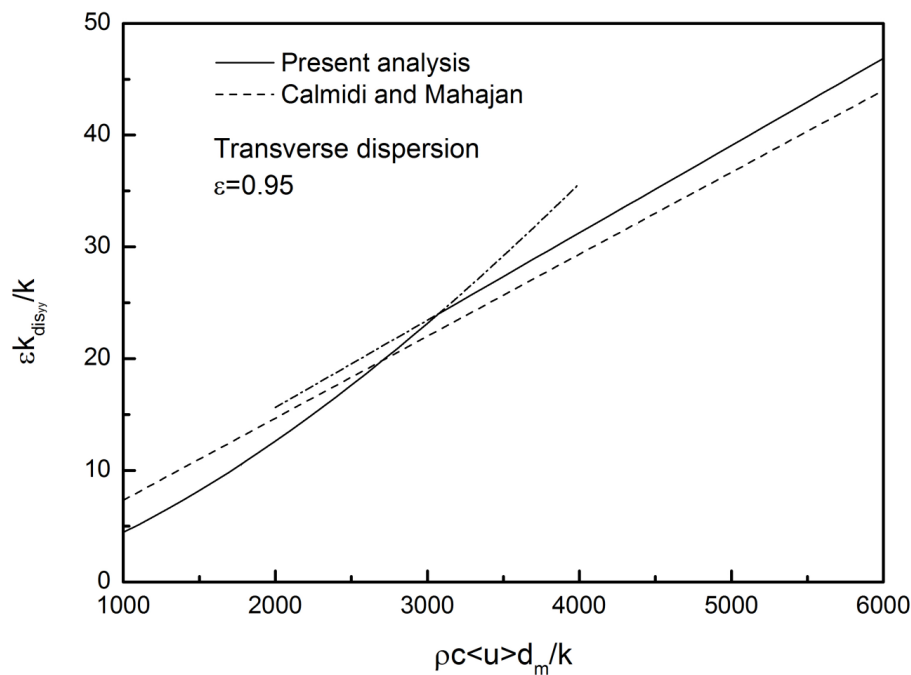


Figure 9. Transverse thermal dispersion in nanofluid saturated metal foam: comparison of empirical correlation and present formulas.

7. Nanoparticle Mechanical Dispersion

For the first time, we shall introduce a mathematical model for the nanoparticle mechanical dispersion. The nanoparticle conservation Equation (37) at steady state is written along the macroscopic flow direction x , as

$$\frac{\partial \langle u \rangle \langle \phi \rangle^f}{\partial x} = \frac{\partial}{\partial x} \left(\epsilon D_B \frac{\partial \langle \phi \rangle^f}{\partial x} + \frac{\epsilon^* D_T}{\langle T \rangle^f} \frac{\partial \langle T \rangle^f}{\partial x} - \epsilon \langle \tilde{\phi} \tilde{u} \rangle^f \right) \tag{61}$$

As illustrated in Figure 8, we consider nanoparticle conservation along a pore scale conduit with its diameter d_m . Thus, nanoparticle mechanical dispersion flux $-\epsilon \langle \tilde{\phi} \tilde{u} \rangle^f$ can be expressed as

$$-\epsilon \langle \tilde{\phi} \tilde{u} \rangle^f = -\langle u \rangle \langle \phi \rangle^f \langle (f - 1) (G - 1) \rangle^f \tag{62}$$

where

$$\phi = \langle \phi \rangle^f G(\eta) \tag{63}$$

Function $G(\eta)$ for the nanoparticle profile may be estimated by solving Equation (4) in a pore conduit:

$$D_B \frac{d\phi}{dr} + \frac{D_T}{T} \frac{dT}{dr} = 0 \tag{64}$$

which can easily be solved with Equations (6a) and (6b) being substituted:

$$\frac{\phi(\eta)}{\phi(1)} = \exp\left(\frac{D_T}{\phi D_B}\Big|_{\eta=1} \left(\frac{\langle T \rangle^s}{T(\eta)} - 1\right)\right) \cong 1 + \frac{\langle T \rangle^s - \langle T \rangle^f}{\langle T \rangle^s} \frac{D_T}{\phi D_B}\Big|_{\eta=1} g(\eta) \tag{65}$$

since $(\langle T \rangle^s - \langle T \rangle^f) / \langle T \rangle^s \ll 1$. Thus,

$$G(\eta) = \frac{\phi(1)}{\langle \phi \rangle^f} \left(1 + \frac{\langle T \rangle^s - \langle T \rangle^f}{\langle T \rangle^s} \frac{D_T}{\phi D_B}\Big|_{\eta=1} g(\eta)\right) = \frac{1 + \frac{\langle T \rangle^s - \langle T \rangle^f}{\langle T \rangle^s} \frac{D_T}{\phi D_B}\Big|_{\eta=1} g(\eta)}{1 + \frac{\langle T \rangle^s - \langle T \rangle^f}{\langle T \rangle^s} \frac{D_T}{\phi D_B}\Big|_{\eta=1}} \tag{66}$$

Using Equation (46a,b) for velocity and temperature profiles, respectively, we readily obtain

$$\langle (f - 1)(G - 1) \rangle^f = \frac{3}{8(1 + n_{BT})} \cong \frac{3}{8n_{BT}} \tag{67}$$

Thus

$$-\varepsilon \langle \tilde{\phi} \tilde{u} \rangle^f = -\frac{3}{8n_{BT}} \langle u \rangle \langle \phi \rangle^f \tag{68}$$

where

$$n_{BT}(\langle T \rangle^f, \langle T \rangle^s) = \frac{\langle T \rangle^s}{\langle T \rangle^s - \langle T \rangle^f} \frac{\phi D_B}{D_T}\Big|_{\eta=1} \tag{69}$$

is a dimensionless function of local volume averaged temperatures, describing the ratio of Brownian and thermophoretic diffusions within a pore conduit, as introduced by Yang *et al.* [23]. Note that absolute value of n_{BT} in most cases is very large, and that, under local thermal equilibrium condition, namely, $\langle T \rangle^s = \langle T \rangle^f$, grows infinitely. Equation (68) may be substituted into Equation (61) to yield

$$\frac{\partial \langle u \rangle \langle \phi \rangle^f}{\partial x} \cong \frac{1}{1 + \frac{3}{8n_{BT}}} \frac{\partial}{\partial x} \left(\varepsilon D_B \frac{\partial \langle \phi \rangle^f}{\partial x} + \frac{\varepsilon^* D_T}{\langle T \rangle^f} \frac{\partial \langle T \rangle^f}{\partial x} \right) \tag{70}$$

Hence, nanoparticle mechanical dispersion works either to suppress or to enhance effective diffusion, as can be seen from the denominator $(1 + 3/8n_{BT})$. It suppresses effective diffusion where the local temperature of metal foam phase is higher than that of nanofluid phase (*i.e.*, $n_{BT} > 0$). On the other hand, it enhances the diffusion where the local temperature of metal foam phase is lower than that of nanofluid phase (*i.e.*, $n_{BT} < 0$). However, this effect of nanoparticle mechanical dispersion on the effective diffusion is limited only to a moderate range of n_{BT} , where local thermal non-equilibrium is discernible. In the region where n_{BT} is very large under nearly local thermal equilibrium, the nanoparticle mechanical dispersion flux $-\varepsilon \langle \tilde{\phi} \tilde{u} \rangle^f$, vanishes, and only stagnant particle diffusion remains. In this way, nanoparticle mechanical dispersion flux varies across the channel, depending on the degree of local thermal non-equilibrium there.

We shall again consider the nanoparticle conservation Equation (37) close enough to the wall surface for convection to be negligible:

$$\frac{\partial}{\partial y} \left(\varepsilon D_B \frac{\partial \langle \phi \rangle^f}{\partial y} + \frac{\varepsilon^* D_T}{\langle T \rangle^f} \frac{\partial \langle T \rangle^f}{\partial y} - \varepsilon \langle \tilde{\phi} \tilde{v} \rangle^f \right) \cong \frac{\partial}{\partial y} \left(\varepsilon D_B \frac{\partial \langle \phi \rangle^f}{\partial y} + \frac{\varepsilon^* D_T}{\langle T \rangle^f} \frac{\partial \langle T \rangle^f}{\partial y} \right) \cong 0 \tag{71}$$

The nanoparticle mechanical dispersion flux $-\varepsilon \langle \tilde{\phi} \tilde{v} \rangle^f$ near the wall surface may be estimated as follows:

$$-\varepsilon \langle \tilde{\phi} \tilde{v} \rangle^f = -\varepsilon \langle \tilde{\phi} \tilde{u} \rangle^f \frac{\langle F(G-1) \rangle^f}{\langle (f-1)(G-1) \rangle^f} \sim \frac{\langle u \rangle \langle \phi \rangle^f}{120n_{BT}} \tag{72}$$

Thus, the transverse nanoparticle mechanical dispersion is so small that it can totally be neglected, irrespective of the degree of local thermal non-equilibrium. Due to no-flux condition at the wall, Equation (71) naturally reduces to

$$\varepsilon D_B \frac{\partial \langle \phi \rangle^f}{\partial y} + \frac{\varepsilon^* D_T}{\langle T \rangle^f} \frac{\partial \langle T \rangle^f}{\partial y} = 0 \tag{73}$$

Unfortunately, no experimental data are available for either transverse or longitudinal coefficients of nanoparticle mechanical dispersion.

8. Mathematical Model for Hydro-Dynamically and Thermally Fully Developed Flows

We shall refer to Figure 10, and consider hydrodynamically and thermally fully developed flows in both channel and tube subject to constant heat flux, filled with a nanofluid saturated metal foam. The walls are subject to axially constant heat flux and circumferentially constant wall temperature (*i.e.*, constant heat flux everywhere).

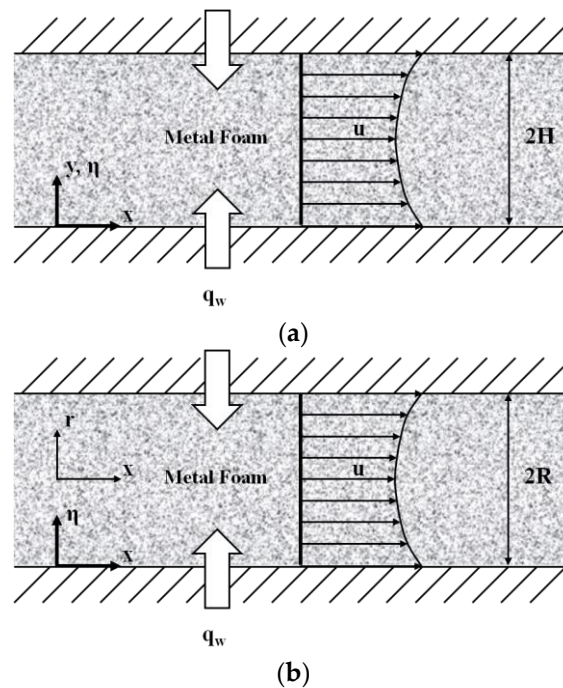


Figure 10. Fully developed flow subject to constant heat flux: (a) channel; and (b) tube. Hydrodynamically and thermally fully developed flow is established in a channel /tube subject to constant heat flux, filled with a nanofluid saturated metal foam, where Darcian velocity is higher close to the wall since the viscosity there is lower.

The macroscopic momentum Equation (34) can be numerically solved along with the macroscopic continuity Equation (33) for the case of fully developed flow in a tube. Such a volume averaged velocity profile is presented in Figure 11, in which the velocity is seen higher close to the wall, since the viscosity there is lower. This overshooting of the velocity works to carry heat effectively away from the heated wall.

In the following analytical treatment, however, the momentum Equation (34) is simplified using Forchheimer extended Darcy law, in which Brinkman term (*i.e.*, macroscopic viscous diffusion term) is dropped, allowing the Darcian velocity slip on the wall. This Forchheimer extended Darcy law is valid

for most of metal foams except for the case of extremely high permeability. Thus, for this case of the channel flow, the volume average Equations (33) to (37) reduce to:

$$-\frac{d\langle p \rangle^f}{dx} = \frac{\mu_f}{K} \langle u \rangle + \rho b \langle u \rangle^2 \tag{74}$$

$$\rho c \langle u \rangle \frac{\partial \langle T \rangle^f}{\partial x} = \frac{\partial}{\partial y} \left(\varepsilon^* k_f + \zeta_k \rho c d_m \langle u \rangle \right) \frac{\partial \langle T \rangle^f}{\partial y} - h_v \left(\langle T \rangle^f - \langle T \rangle^s \right) \tag{75}$$

$$\frac{\partial}{\partial y} \left(1 - \varepsilon^* \right) k_s \frac{\partial \langle T \rangle^s}{\partial y} - h_v \left(\langle T \rangle^s - \langle T \rangle^f \right) = 0 \tag{76}$$

$$\frac{\partial}{\partial y} \left(\varepsilon D_B \frac{\partial \langle \phi \rangle^f}{\partial y} + \frac{\varepsilon^* D_T}{\langle T \rangle^f} \frac{\partial \langle T \rangle^f}{\partial y} \right) = 0 \tag{77}$$

Following Equations (59), transverse thermal dispersion coefficient may be evaluated from

$$\zeta_k = \frac{0.00742}{\varepsilon} \tag{78}$$

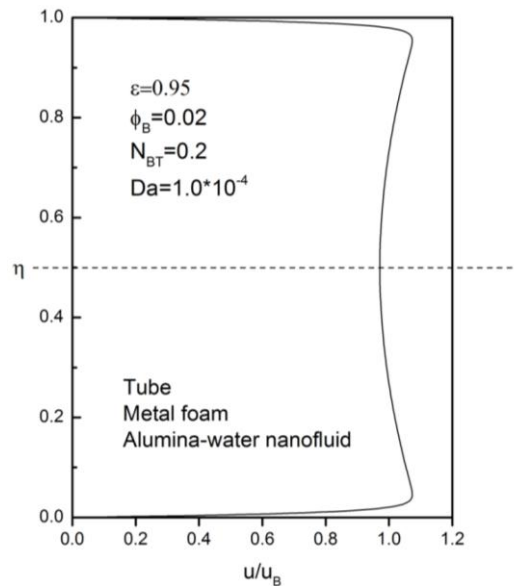


Figure 11. Velocity overshooting in a tube flow: numerical results based on the full momentum equation.

Moreover, the interstitial volumetric coefficient h_v is evaluated from Equation (43). Note that the continuity equation yields $\partial \langle u \rangle / \partial x = 0$ and $\langle v \rangle = 0$.

The origin of vertical coordinate y is set on the lower wall. The boundary conditions are given by

$$q_0 = - \left(\varepsilon^* k_f + \zeta_k \rho c d_m \langle u \rangle \right) \frac{\partial \langle T \rangle^f}{\partial y} \Big|_{y=0} - (1 - \varepsilon^*) k_s \frac{\partial \langle T \rangle^s}{\partial y} \Big|_{y=0} \tag{79}$$

$$\varepsilon D_B \frac{\partial \langle \phi \rangle^f}{\partial y} \Big|_{y=0} + \frac{\varepsilon^* D_T}{\langle T \rangle^f} \frac{\partial \langle T \rangle^f}{\partial y} \Big|_{y=0} = 0 \tag{80}$$

$$\frac{\partial \langle \phi \rangle^f}{\partial y} \Big|_{y=H} = 0 \tag{81a}$$

$$\left. \frac{\partial \langle T \rangle^f}{\partial y} \right|_{y=H} = \left. \frac{\partial \langle T \rangle^s}{\partial y} \right|_{y=H} = 0 \tag{81b}$$

Kuwahara *et al.* [12] considered two extreme cases for possible wall temperature difference between solid and fluid phases, namely, locally uniform heat flux wall and locally thermal equilibrium wall, and concluded that the locally thermal equilibrium wall is much closer to the reality. Hence, we assume:

$$\langle T \rangle^s|_{y=0} = \langle T \rangle^f|_{y=0} \equiv T_0(x) : \text{ wall temperature} \tag{82}$$

where $T_0(x)$ is the wall temperature. $T_0(x)$ increases linearly downstream under constant heat flux. Nanoparticle conservation Equation (77) indicates that diffusion mass flux of nanoparticles is constant across the channel. Since the wall is impermeable, the boundary condition Equation (80) holds such that effective Brownian diffusion flux and effective thermophoretic diffusion flux cancel out everywhere across the channel. Energy Equations (75) and (76) may be added together and integrated over the lower half channel from $y = 0$ to H with boundary conditions Equations (79) and (80) to give

$$\overline{\rho c \langle u \rangle} \frac{dT_B}{dx} = \frac{q_0}{H} \tag{83}$$

where the subscript 0 refers to the wall at $y = 0$, and

$$\bar{\varphi} \equiv \frac{1}{A} \int_A \varphi dA = \frac{1}{H} \int_0^H \varphi dy \tag{84}$$

denotes the average value over the cross-section such that

$$T_B \equiv \frac{\overline{\rho c \langle u \rangle \langle T \rangle}}{\overline{\rho c \langle u \rangle}} \tag{85a}$$

is the bulk mean temperature. Likewise, quantities with subscript B denote bulk quantities such as

$$\phi_B \equiv \overline{\langle u \rangle \langle \phi \rangle^f} / \overline{\langle u \rangle} \tag{85b}$$

$$u_B \equiv \overline{\rho \langle u \rangle} / \rho(\phi_B) \tag{85c}$$

The foregoing considerations on both nanoparticle diffusion flux and axial temperature gradient will be implemented to obtain analytical expressions in a dimensionless form. The momentum Equation (74) may be arranged in a dimensionless form as

$$u^*(y^*) = \frac{\sqrt{1 + 4Da^2Hg \frac{(\rho/\rho_0)}{(\mu/\mu_0)^2}} - 1}{2DaHg \frac{(\rho/\rho_0)}{(\mu/\mu_0)}} \tag{86}$$

Thus, for the case of Forchheimer extended Darcy flow (*i.e.*, $Da \ll 1$), the velocity profile is described algebraically as the viscosity of nanofluid is provided as function of the nanoparticle volume fraction. The other governing equations are given in differential forms as follows:

$$\frac{\rho c u^*}{\rho c u^*} = -\frac{d}{dy^*} \left(\varepsilon^* \frac{k}{k_{stag0}} + \zeta_k Pe \frac{\rho c}{(\rho c)_0} u^* \right) \frac{dT^{*f}}{dy^*} + Nu_v (T^{*f} - T^{*s}) \tag{87}$$

$$(1 - \varepsilon^*) \frac{k_s}{k_{stag0}} \frac{d^2 T^{*s}}{dy^{*2}} - Nu_v (T^{*s} - T^{*f}) = 0 \tag{88}$$

$$\frac{d \langle \phi \rangle^f}{dy^*} = \frac{\varepsilon^* \langle \phi \rangle^f}{\varepsilon N_{BT} (1 - \gamma T^{*f})^2} \frac{dT^{*f}}{dy^*} \tag{89}$$

Dimensionless coordinate, velocity and temperature are defined as

$$y^* = y/H \tag{90}$$

$$u^* = \langle u \rangle / \left(\frac{H^2}{\mu_0} \left(-\frac{d\langle p \rangle^f}{dx} \right) \right) \tag{91a}$$

$$T^{*f} = \frac{k_{stag0} (T_0 - \langle T \rangle^f)}{q_0 H} \tag{91b}$$

$$T^{*s} = \frac{k_{stag0} (T_0 - \langle T \rangle^s)}{q_0 H} \tag{91c}$$

$$N_{BT} \equiv \frac{D_{B0} T_0 \phi_0 k_{stag0}}{D_{T0} q_0 H} = \frac{D_{B0} \phi_0}{D_{T0} \gamma} \tag{92a}$$

$$\gamma \equiv \frac{q_0 H}{k_{stag0} T_0} \tag{92b}$$

Furthermore, Darcy, Lewis, Peclet, and Hagen numbers are defined as follows:

$$Da \equiv K/H^2 \tag{93a}$$

$$Le \equiv k_{stag0} / (\rho c)_0 D_{B0} \tag{93b}$$

$$Pe \equiv \frac{\rho_0 c_0 \sqrt{K} H^2}{k_{stag0} \mu_0} \left(-\frac{d\langle p \rangle^f}{dx} \right) \tag{93c}$$

$$Hg \equiv \frac{\rho_0 b H^4}{\mu_0^2} \left(-\frac{d\langle p \rangle^f}{dx} \right) \tag{93d}$$

where the properties with subscript 0 should be evaluated at the wall according to Equations (5a) to (6b), (30) and (31). For example, the stagnation thermal conductivity at wall where $\langle \phi \rangle^f|_{y^*=0} = \phi_0$ may be evaluated according to Equations (5d), (30) and (31) as

$$k_{stag0} = \varepsilon * k|_{y^*=0} + (1 - \varepsilon *) k_s = \frac{2 + \varepsilon}{3} \left(1 + 2.72\phi_0 + 4.97\phi_0^2 \right) k_{bf} + \frac{1 - \varepsilon}{3} k_s \tag{94}$$

The dimensionless parameter N_{BT} is related to the ratio of macroscopic Brownian and thermophoretic diffusivities. N_{BT} can range over a wide range from 0.1 to 10 for typical cases of alumina and copper nanoparticles with $d_p \sim 10$ nm and the bulk mean particle volume fraction $\phi_B \sim 0.01$. The ratio of wall and fluid temperature difference to absolute temperature, namely, $\gamma \sim (T_0 - \langle T \rangle_B^f) / T_0$, is usually much smaller than unity, as estimated by Buongiorno [17]. Similarity between “microscopic” ratio n_{BT} (Equation (69)) and “macroscopic” ratio N_{BT} (Equation (92a)) is worth noting, since the former describes the local ratio of microscopic Brownian and thermophoretic diffusivities in a pore scale, whereas the latter describes the ratio of macroscopic Brownian and thermophoretic diffusivities in a channel filled with a nanofluid saturated metal foam.

In reality, the bulk mean particle volume fraction ϕ_B is given, while that at the wall ϕ_0 is unknown. However, for the sake of computational convenience, ϕ_0 is prescribed and ϕ_B is calculated later to find out ϕ_0 as a function of ϕ_B .

The energy Equations (87) and (88) can be combined to form a third order Ordinary Differential Equation (O.D.E.) with respect to T^{*s} as

$$\frac{d^3 T^{*s}}{dy^{*3}} = Nu_v \frac{\left(\frac{k_{stag}}{k_{stag0}} + \zeta_k Pe \frac{\rho c}{(\rho c)_0} u^* \right) \frac{dT^{*s}}{dy^*} - \int_{\eta}^1 \frac{\rho c u^*}{\rho c u^*} dy^*}{\left(\varepsilon^* \frac{k_f}{k_{stag0}} + \zeta_k Pe \frac{\rho c}{(\rho c)_0} u^* \right) (1 - \varepsilon^*) \frac{k_s}{k_{stag0}}} \tag{95}$$

where

$$T^{*f} = T^{*s} - \frac{(1 - \varepsilon^*)}{Nu_v} \frac{k_s}{k_{stag0}} \frac{d^2 T^{*s}}{dy^{*2}} \tag{96}$$

and Equation (89) can easily be integrated with $\langle \phi \rangle^f \Big|_{y^*=0} = \phi_0$ to obtain

$$\frac{\langle \phi \rangle^f}{\phi_0} = \exp \left(\frac{\varepsilon^* T^{*f}}{N_{BT} \varepsilon (1 - \gamma T^{*f})} \right) \tag{97}$$

The foregoing third order O.D.E. Equation (95) may easily be solved by using a standard integration scheme such as Runge–Kutta–Gill method (e.g., [21]). Appropriate boundary conditions for the equation are given by

$$T^{*s} \Big|_{y^*=0} = \frac{d^2 T^{*s}}{dy^{*2}} \Big|_{y^*=0} = 0 \tag{98a}$$

$$\text{and } \frac{dT^{*s}}{dy^*} \Big|_{y^*=1} = 0 \tag{98b}$$

which are based on the original boundary conditions given by Equations (81b) and (82).

A similar procedure based on the cylindrical coordinate system as shown in Figure 10b readily yields the following set of transformed equations for the case of circular tube:

$$\frac{d^3 T^{*s}}{dy^{*3}} - \frac{1}{1 - y^*} \frac{d^2 T^{*s}}{dy^{*2}} - \frac{1}{(1 - y^*)^2} \frac{dT^{*s}}{dy^*} = Nu_v \frac{\left(\frac{k_{stag}}{k_{stag0}} + \zeta_k Pe \frac{\rho_f c_f}{\rho_f c_{f0}} u^* \right) \frac{dT^{*s}}{dy^*} - \frac{2}{1 - y^*} \int_{y^*}^1 \frac{\rho_f c_f u^*}{\rho c u^*} (1 - y^*) dy^*}{\left(\varepsilon^* \frac{k_f}{k_{stag0}} + \zeta_k Pe \frac{\rho_f c_f}{\rho_f c_{f0}} u^* \right) (1 - \varepsilon^*) \frac{k_s}{k_{stag0}}} \tag{99}$$

where

$$T^{*f} = T^{*s} - \frac{(1 - \varepsilon^*)}{Nu_v} \frac{k_s}{k_{stag0}} \left(\frac{d^2 T^{*s}}{dy^{*2}} - \frac{1}{1 - y^*} \frac{dT^{*s}}{dy^*} \right) \tag{100}$$

The boundary conditions in the cylindrical coordinate are the same as those given by Equation (98a,b). Moreover, Equation (97) for the volume averaged nanoparticle volume fraction holds also for the case of cylindrical coordinate system. However, note that the average value $\bar{\varphi}$ for the case of the tube is computed by

$$\bar{\varphi} \equiv \frac{1}{A} \int_A \varphi dA = \frac{1}{\pi R^2} \int_0^R 2\pi r \varphi dr = 2 \int_0^1 (1 - y^*) \varphi dy^* \tag{101}$$

where $y^* = (R - r)/R$. The corresponding dimensionless quantities u^* to Nu_v are defined just as presented in Equations (91a) to (93d) replacing the channel half height H by the tube radius R .

9. Results and Discussion

The foregoing set of equations may be integrated numerically using the Runge–Kutta–Gill method for the case of channel with $\varepsilon = 0.9$, $Da = 10^{-4}$, $N_{BT} = 0.5$ and $\phi_B = 0.02$. Figure 12 shows the effects of the interstitial Nusselt number Nu_v on fluid and solid temperature profiles.

The temperature profile of nanofluid and that of metal foam tend to get closer each other for sufficiently large Nu_v , in which local thermal equilibrium holds. Usually, the solid temperature is

higher than the nanofluid temperature (i.e., $T^{*s} = k_{stag0} (T_0 - \langle T \rangle^s) / q_0 H$ is smaller and flatter than $T^{*f} = k_{stag0} (T_0 - \langle T \rangle^f) / q_0 H$).

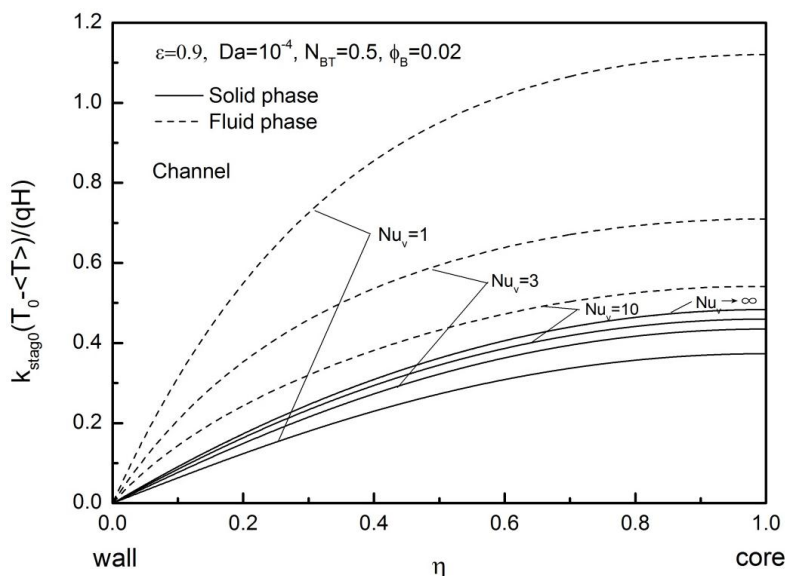


Figure 12. Effects of Nu_v on the temperature profiles in a channel filled with a nanofluid saturated metal foam.

The corresponding particle volume fraction and velocity profiles in the channel are shown in Figures 13 and 14 respectively. The nanoparticle volume fraction distribution becomes somewhat flatter as increasing Nu_v , since the nanofluid temperature tends to follow the solid temperature, as witnessed in Figure 13. As can be seen from Figure 13, the nanoparticle volume fraction gradually converges to a profile corresponding to the case of $Nu_v \rightarrow \infty$. Figure 14 clearly shows that the velocity is higher near the heated wall where viscosity is less, as thermophoretic diffusion dominates over Brownian diffusion, driving nanoparticles away from the wall.

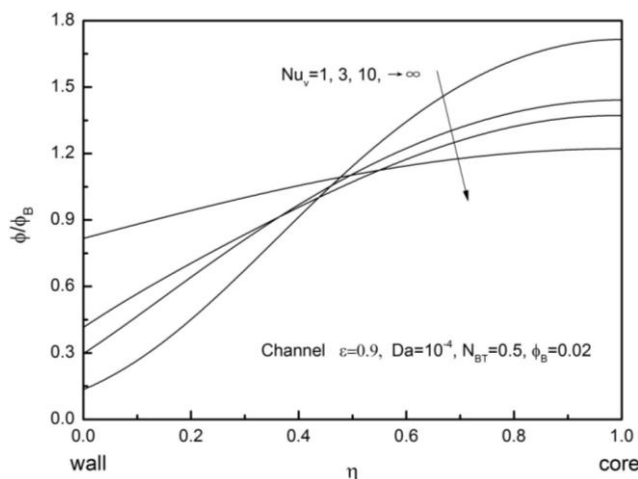


Figure 13. Effects of Nu_v on the nanoparticle distribution in a channel filled with a nanofluid saturated metal foam.

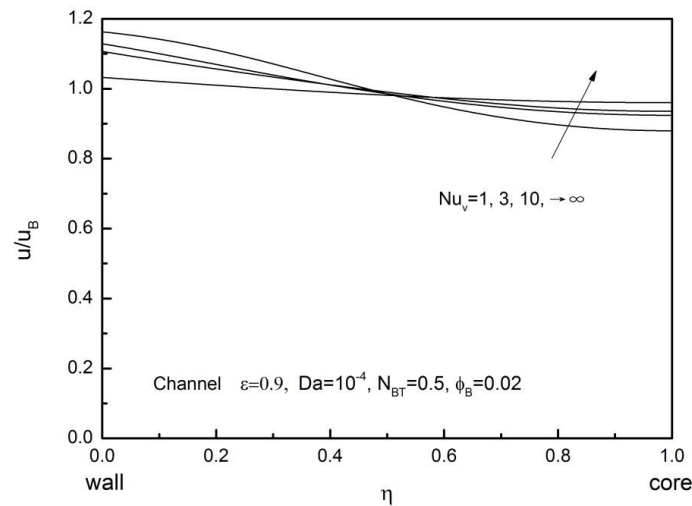


Figure 14. Effects of Nu_v on the velocity distribution in a channel filled with a nanofluid saturated metal foam.

By changing the value N_{BT} , another series of computations were conducted with $\epsilon = 0.9$, $Da = 10^{-4}$, $Nu_v = 1$ and $\phi_B = 0.02$, so as to investigate the effect of the ratio of macroscopic Brownian and thermophoretic diffusivities, N_{BT} , on nanoparticle volume fraction profile, velocity profile and both fluid and solid temperature profiles.

As shown in Figure 15, the nanoparticle volume fraction becomes uniform for large N_{BT} . Because Brownian diffusion dominates over thermophoretic diffusion, nanoparticles are dispersed evenly for large N_{BT} . Figure 16 shows that the velocity profile becomes completely flat under such a uniform nanoparticle volume fraction distribution, resulting in a plug flow.

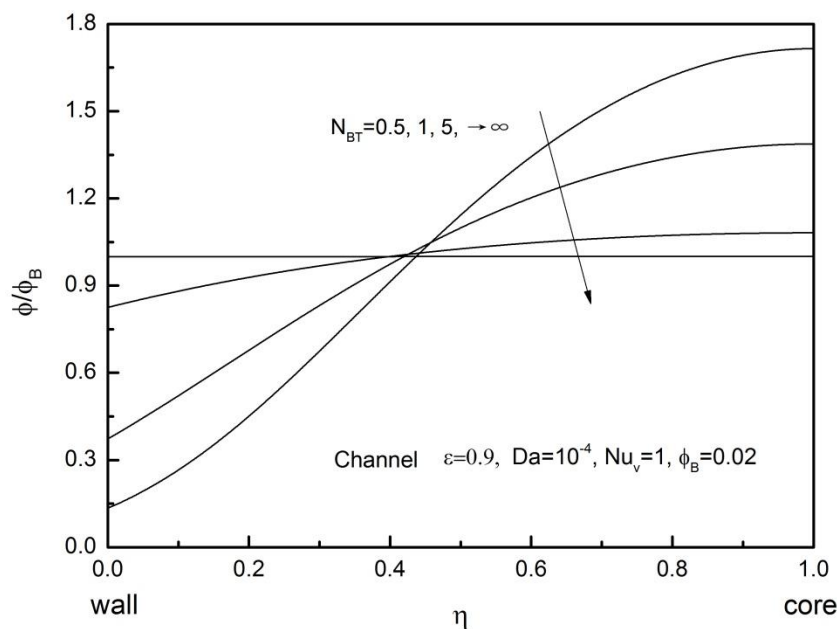


Figure 15. Effects of N_{BT} on the nanoparticle volume fraction distribution in a channel filled with a nanofluid saturated metal foam.

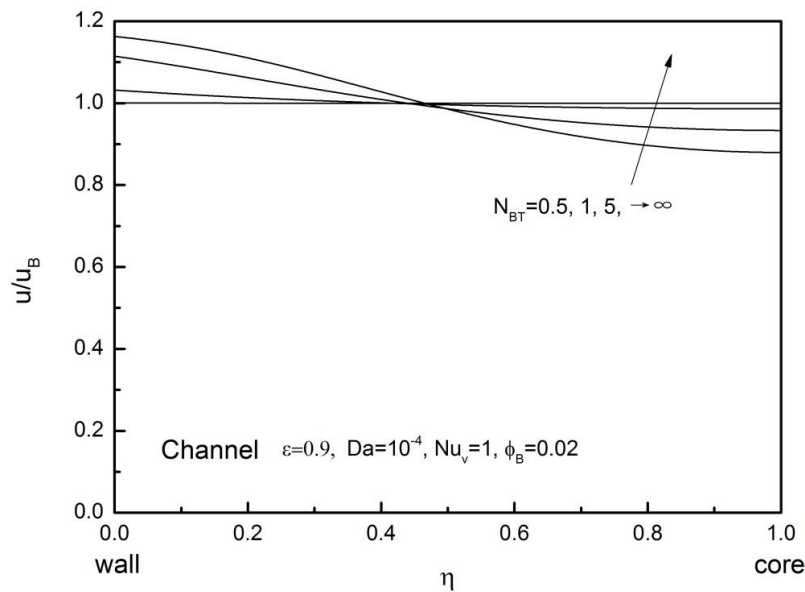


Figure 16. Effects of N_{BT} on the velocity distribution in a channel filled with a nanofluid saturated metal foam.

In Figure 17, both nanofluid temperature and metal foam temperature are plotted for a range of N_{BT} . Nu_v is only at a moderate level such that a substantial difference can be observed between two temperatures. As can be confirmed from the figure, however, the effects of N_{BT} on the temperature profiles are rather limited.

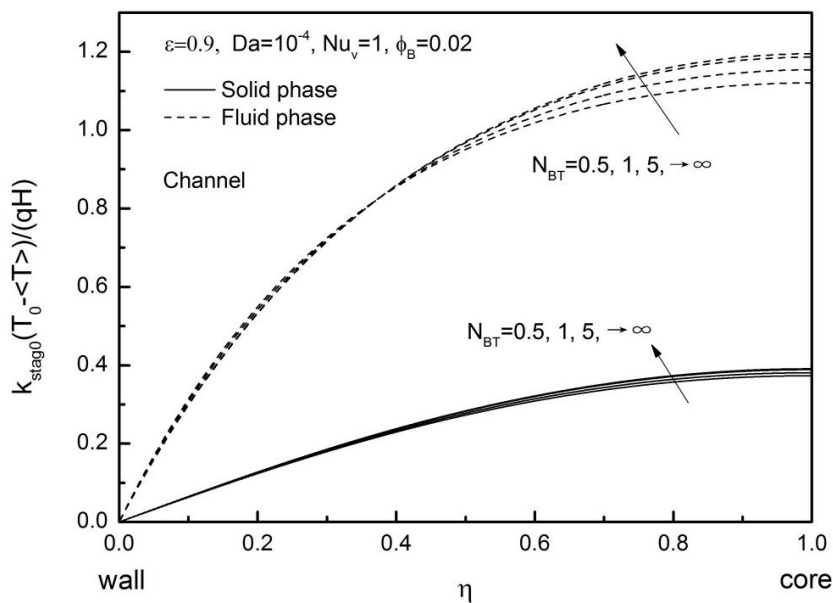


Figure 17. Effects of N_{BT} on the temperature distribution in a channel filled with a nanofluid saturated metal foam.

9.1. Asymptotic Solutions for the Case of Nearly Uniform Nanoparticle Distribution ($N_{BT} \gg 1$)

Brownian diffusion overwhelms thermophoretic diffusion for the case of sufficiently small nanoparticle diameter, such that its macroscopic ratio N_{BT} becomes much greater than unity. Equation (97) under such cases yields

$$\frac{\langle \phi \rangle^f}{\phi_0} = \exp\left(\frac{\varepsilon^* T^{*f}}{N_{BT} \varepsilon (1 - \gamma T^{*f})}\right) \cong 1 + \frac{\varepsilon^*}{N_{BT} \varepsilon} T^{*f} \tag{102}$$

where $\gamma \ll 1$. The foregoing equation indicates that the profile of volume averaged nanoparticle volume fraction $\langle \phi \rangle^f (y^*)$ becomes similar to that of nanofluid phase temperature $T^{*f} (y^*)$. Moreover, it tends to be uniform for sufficiently large N_{BT} , as consistently observed in Figure 15. Under such uniform distribution of volume averaged nanoparticle volume fraction, all thermophysical properties become uniform across the channel.

9.1.1. Channel Flows

Thus, the third order O.D.E. Equation (91) and nanofluid temperature Equation (96) with the boundary conditions Equations (98a) and (98b) yields the following analytic solutions:

$$T^{*s} = \frac{y^* - \frac{1}{2}y^{*2} - \frac{1}{\zeta^2} \left(1 - \frac{\cosh(\zeta(1-y^*))}{\cosh\zeta}\right)}{1 + \zeta_k Pe u_B^*} \tag{103}$$

and

$$T^{*f} = \frac{y^* - \frac{1}{2}y^{*2} + \frac{1 - \varepsilon^* \frac{k(\phi_B)}{k_{stag0}}}{\left(\varepsilon^* \frac{k(\phi_B)}{k_{stag0}} + \zeta_k Pe u_B^*\right) \zeta^2} \left(1 - \frac{\cosh(\zeta(1-y^*))}{\cosh\zeta}\right)}{1 + \zeta_k Pe u_B^*} \tag{104}$$

where

$$\zeta = \sqrt{\frac{1 + \zeta_k Pe u_B^*}{(1 - \varepsilon^*) \frac{k_s}{k_{stag0}} \left(\varepsilon^* \frac{k(\phi_B)}{k_{stag0}} + \zeta_k Pe u_B^*\right)}} Nu_v \tag{105a}$$

and

$$u_B^* = \frac{\sqrt{1 + 4Da^2Hg} - 1}{2DaHg} \tag{105b}$$

Nusselt number of our interest is given by

$$Nu_H = \frac{q_0 H}{k(\phi_B)(T_0 - T_B)} = \frac{1}{\frac{k(\phi_B)}{k_{stag0}} T_B^*} = \frac{1}{\frac{k(\phi_B)}{k_{stag0}} T^{*f}} = \frac{k_{stag0}}{k(\phi_B)} \frac{1 + \zeta_k Pe u_B^*}{\frac{1}{3} + \frac{1 - \frac{2 + \varepsilon k(\phi_B)}{3 k_{stag0}}}{\left(\frac{2 + \varepsilon k(\phi_B)}{3 k_{stag0}} + \zeta_k Pe u_B^*\right) \zeta^2} \left(1 - \frac{\tanh\zeta}{\zeta}\right)} \tag{106}$$

The ratio of heat transfer coefficient for convection in a nanofluid saturated metal foam to that for the case of base fluid convection without a metal foam is given by

$$\frac{h(\phi_B)}{h_{bf}} = \frac{4}{(140/17)} \frac{k_{stag0}}{k_{bf}} \frac{1 + \zeta_k Pe u_B^*}{1 - \frac{2 + \varepsilon k(\phi_B)}{3 k_{stag0}} \frac{1}{\left(\frac{2 + \varepsilon k(\phi_B)}{3 k_{stag0}} + \zeta_k Pe u_B^*\right) \zeta^2} \left(1 - \frac{\tanh\zeta}{\zeta}\right)} \tag{107}$$

9.1.2. Tube Flows

The corresponding set of solutions for the case of tubes may be obtained by solving Equation (99) as

$$T^{*s} = \frac{y^* - \frac{1}{2}y^{*2} - \frac{2}{\zeta^2} \left(1 - \frac{I_0(\zeta(1-y^*))}{I_0(\zeta)} \right)}{1 + \zeta_k Pe u_B^*} \tag{108}$$

where I_0 is the modified zero order Bessel function of the first kind. The dimensionless nanofluid temperature is obtained substituting Equations (108) into (100) as

$$T^{*f} = \frac{y^* - \frac{1}{2}y^{*2} + \frac{2 \left(1 - \varepsilon^* \frac{k(\phi_B)}{k_{stag0}} \right)}{\left(\varepsilon^* \frac{k(\phi_B)}{k_{stag0}} + \zeta_k Pe u_B^* \right) \zeta^2} \left(1 - \frac{I_0(\zeta(1-y^*))}{I_0(\zeta)} \right)}{1 + \zeta_k Pe u_B^*} \tag{109}$$

where the dimensionless bulk velocity is given by Equation (105b). The corresponding Nusselt number may be numerically evaluated as

$$Nu_R = \frac{q_0 R}{k(\phi_B)(T_0 - T_B)} = \frac{1}{\frac{k(\phi_B)}{k_{stag0}} T_B^*} = \frac{1}{\frac{k(\phi_B)}{k_{stag0}} T^{*f}} \tag{110}$$

The ratio of heat transfer coefficient for convection in a nanofluid saturated metal foam to that for the case of base fluid convection without a metal foam is given by

$$\frac{h(\phi_B)}{h_{bf}} = \frac{2}{(48/11)} \frac{k_{stag0}}{k_{bf}} \frac{1}{T^{*f}} \tag{111}$$

9.2. Asymptotic Solutions for the Case of Nearly Local Thermal Equilibrium ($Nu_v \gg 1$)

Equation (96) for the channel flow case and Equation (100) for the tube flow case clearly indicate $T^{*f} \cong T^{*s}$ when the interstitial volumetric coefficient is sufficiently high (i.e., $Nu_v \gg 1$). Thus, local thermal equilibrium holds everywhere over the cross-section.

9.2.1. Channel Flows

Equation (87) readily yields analytic solutions.

$$T^{*f} \cong T^{*s} = \int_0^{y^*} \frac{\int_{y^*}^1 \frac{\rho c u^*}{\rho c u^*} dy^*}{\frac{k_{stag}}{k_{stag0}} + \zeta_k Pe \left(\frac{\rho c}{\rho_0 c_0} \right) u^*} dy^* \tag{112}$$

This integral equation can be approximated very well by

$$T^{*f} \cong T^{*s} = \frac{y^* - \frac{1}{2}y^{*2}}{\frac{k_{stag}(\phi_B)}{k_{stag0}} + \zeta_k Pe \frac{\sqrt{1 + 4Da^2Hg} - 1}{2DaHg}} \tag{113}$$

Substitution of the foregoing temperature profile into Equation (97) readily gives the profile of volume averaged nanoparticle volume fraction. The corresponding Nusselt number is given by

$$Nu_H = \frac{q_0 H}{k(\phi_B)(T_0 - T_B)} = \frac{1}{\frac{k(\phi_B)}{k_{stag0}} T_B^*} = \frac{1}{\frac{k(\phi_B)}{k_{stag0}} T^{*f}} = 3 \left(1 + \frac{k_{stag0}}{k(\phi_B)} \zeta_k Pe \frac{\sqrt{1 + 4Da^2Hg} - 1}{2DaHg} \right) \tag{114}$$

The ratio of heat transfer coefficient for convection in a nanofluid saturated metal foam to that for the case of base fluid convection without a metal foam is given by

$$\frac{h(\phi_B)}{h_{bf}} = \frac{12}{(140/17)} \left(\frac{k(\phi_B)}{k_{bf}} + \frac{k_{stag0}}{k_{bf}} \zeta_k Pe \frac{\sqrt{1 + 4Da^2Hg} - 1}{2DaHg} \right) \tag{115}$$

9.2.2. Tube Flows

The corresponding set of the solutions for the case of tubes may be obtained from Equation (99) as

$$T^{*f} \cong T^{*s} = \int_0^{y^*} \frac{\int_{y^*}^1 2(1-y^*) \frac{\rho c u^*}{\rho c u^*} d\eta}{(1-y^*) \left(\frac{k_{stag}}{k_{stag0}} + \zeta_k Pe \left(\frac{\rho c}{\rho_0 c_0} \right) u^* \right)} dy^* \tag{116}$$

which may well be approximated by

$$T^{*f} \cong T^{*s} = \frac{y^* - \frac{1}{2}y^{*2}}{\frac{k_{stag}(\phi_B)}{k_{stag0}} + \zeta_k Pe \frac{\sqrt{1 + 4Da^2Hg} - 1}{2DaHg}} \tag{117}$$

Thus, the profile of volume averaged temperature given by Equation (117) and that of nanoparticle volume fraction given by its substitution into Equation (97) for the tube are similar to those for the channel. Accordingly, Nusselt number for the tube is given by

$$Nu_R = \frac{q_0 R}{k(\phi_B)(T_0 - T_B)} = \frac{1}{\frac{k(\phi_B)}{k_{stag0}} T_B^*} = \frac{1}{\frac{k(\phi_B)}{k_{stag0}} \frac{T^{*f}}{T_B^*}} = 4 \left(1 + \frac{k_{stag0}}{k(\phi_B)} \zeta_k Pe \frac{\sqrt{1 + 4Da^2Hg} - 1}{2DaHg} \right) \tag{118}$$

The ratio of heat transfer coefficient for convection in a nanofluid saturated metal foam to that for the case of base fluid convection without a metal foam is given by

$$\frac{h(\phi_B)}{h_{bf}} = \frac{8}{(48/11)} \left(\frac{k_{stag}(\phi_B)}{k_{bf}} + \frac{k_{stag0}}{k_{bf}} \zeta_k Pe \frac{\sqrt{1 + 4Da^2Hg} - 1}{2DaHg} \right) \tag{119}$$

Heat transfer enhancement in a nanoparticle saturated metal foam can be partly due to an increase in its stagnant thermal conductivity, which results from both highly conductive nanoparticles and consolidated metal foam, and partly due to intensified nanofluid mixing resulting from mechanical dispersion within a foam. This enhancement can best be illustrated in the foregoing Equation (119). The first term in the right hand side gives the heat transfer rate increase due to embedding of metal foam and addition of nanoparticles, while the second term describes heat transfer enhancement due to thermal dispersion.

9.3. Heat Transfer Performance Evaluation

Figure 18 shows heat transfer coefficient ratios $h(\phi_B)/h_{bf}$ for given ϕ_B against a dimensionless pumping power:

$$P.P.(Hg; Da) \equiv \left(-\frac{d\langle p \rangle^f}{dx} u_B \right) \left(\frac{\rho_0^2 b^2 R^6}{\mu_0^3} \right) = \frac{\sqrt{1 + 4Da^2Hg} - 1}{2Da} Hg \tag{120}$$

$h(\phi_B)/h_{bf}$ is plotted in a possible range of $P.P. = 6.0 \times 10^9 - 1.3 \times 10^{15}$ (corresponding to $\langle u \rangle = 0.01$ to 1 m/s, $2R = 0.02$ m, $d_m = 0.001$ m) for the tube. The figure clearly indicates that heat transfer coefficient for the tube filled with a nanofluid saturated metal foam is much higher than that

for a tube filled with a base fluid. The ratio increases towards 80 as increasing the pumping power $P.P.$, in which thermal dispersion becomes significant. Naturally, higher volume fraction of nanofluid results in higher heat transfer coefficient, especially when $P.P.$ is large such that thermal dispersion is quite significant.

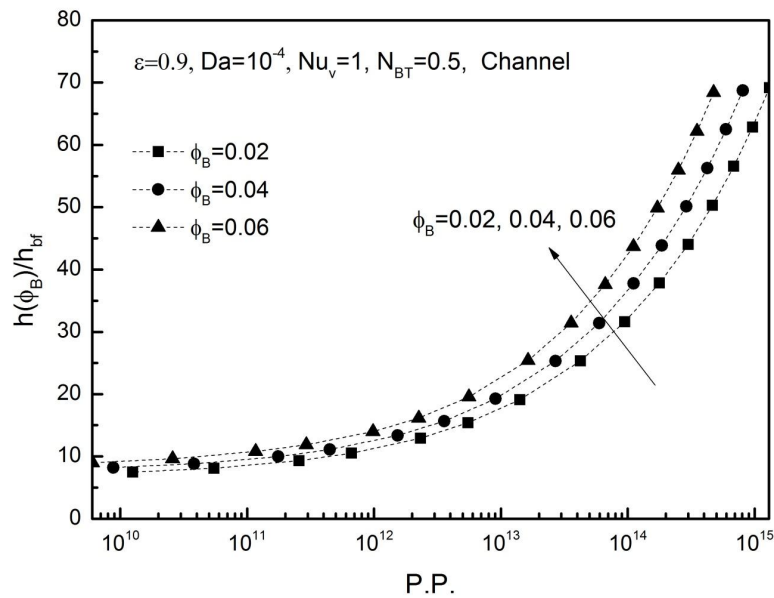


Figure 18. Effects of ϕ_B on the heat transfer coefficient ratio in a channel filled with a nanofluid saturated metal foam.

Figure 19 shows the effects of N_{BT} on the heat transfer ratio $h(\phi_B)/h_{bf}$. As expected from Figure 17 showing the temperature profiles, which are fairly insensitive to N_{BT} , the heat transfer ratios obtained with different values of N_{BT} almost coincide one another. Figure 20, on the other hand, shows effects of Nu_v on the heat transfer coefficient ratio $h(\phi_B)/h_{bf}$, which clearly indicates that higher interstitial heat transfer coefficient yields higher macroscopic heat transfer coefficient. Therefore, combination of metal foams and nanofluids is believed to bring unconventionally high heat transfer coefficients.

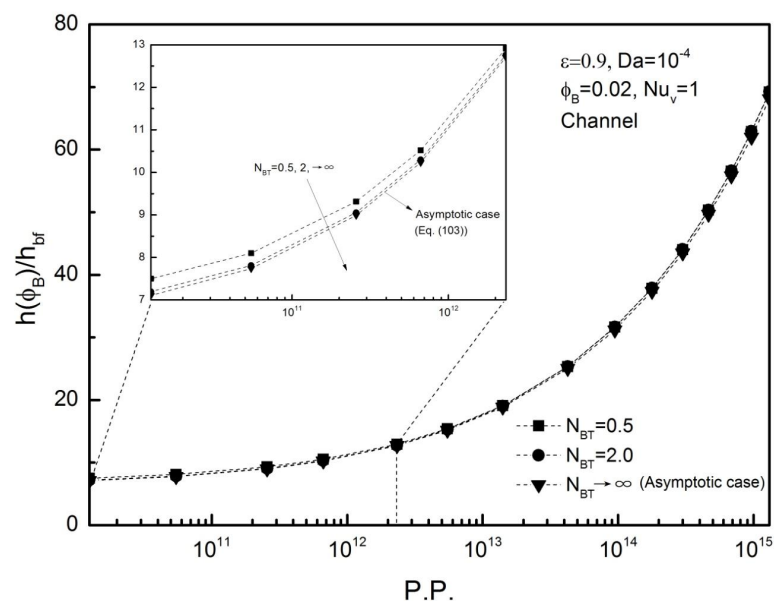


Figure 19. Effects of N_{BT} on the heat transfer coefficient ratio in a channel filled with a nanofluid saturated metal foam.

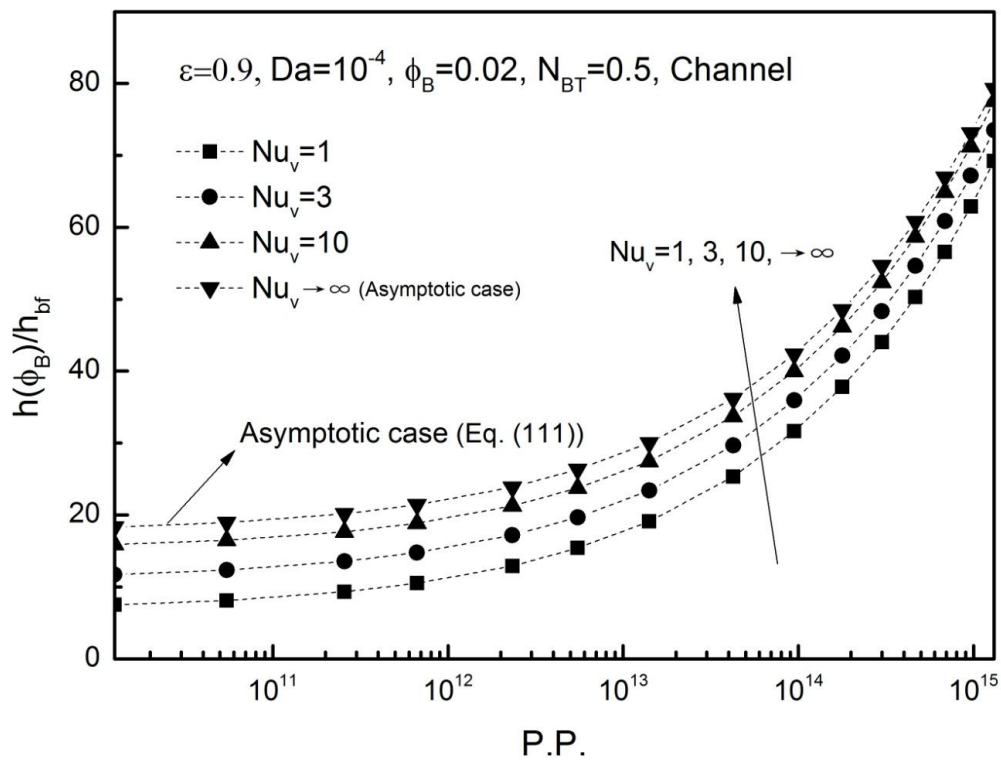
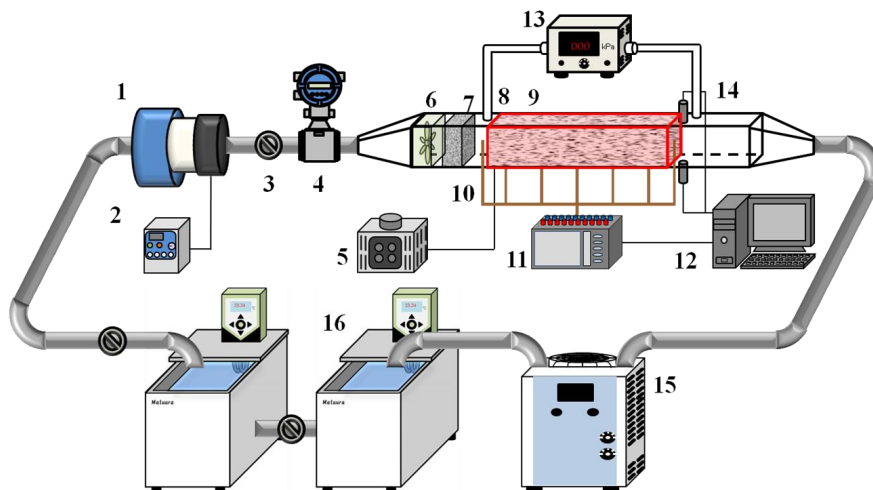


Figure 20. Effects of Nu_v on the heat transfer coefficient ratio in a channel filled with a nanofluid saturated metal foam.

The experimental verification is underway using the experimental set-up, as shown in Figure 21. The experimental results obtained from the program partially supported by the JSPS Grants-in-Aid for Scientific Research B, will be available near future.



1. Pump, 2. Inverter, 3. Control valve, 4. Flow meter, 5. Transformer, 6. Fan, 7. Filter, 8. Heater, 9. Metal foam, 10. Thermocouples, 11. Data logger, 12. Computer, 13., 14. Pressure gauge, 15. Ultrasonic velocimeter, 16. Bath

Figure 21. Experimental set-up for heat transfer measurement.

10. Concluding Remarks

A rigorous derivation of the macroscopic governing equations was presented for analyzing convective heat transfer in nanofluid saturated metal foam. A volume averaging theory was introduced

to integrate the microscopic set of the modified Buongiorno equations over a local control volume. The unknown correlation terms resulting from the volume averaging were mathematically modeled so as to close the set of governing equations. A pore scale conduit model was used to investigate both thermal dispersion term and particle mechanical dispersion term analytically. Upon assuming microscopic distribution profiles for velocity and temperature within a pore, dispersion coefficients were evaluated for thermal dispersion and particle mechanical dispersion. The present analytical expression for the transverse thermal dispersion based on the pore scale analysis was found to closely follow the Calmid–Mahajan empirical correlation. The longitudinal particle mechanical dispersion was found to work either to suppress or to enhance effective diffusion depending on the sign of local phase temperature difference, while the transverse counterpart is insignificant and therefore can be neglected. Moreover, it has been found, conducting a comparison under equal pumping power, that a high level of the heat transfer rate (about 80 times more than the case of base fluid convection without a metal foam) is possible using a combination of metal foam and nanofluid. Thus, we can conclude that the nanofluid saturated metal foams can be utilized for conceiving a new generation of high performance heat exchangers.

It should finally be pointed out that possible nanofluid fouling due to nanoparticles coagulation on the internal wall of solid matrix has been neglected in this study. Sarafraz *et al.* [41] conducted experiments to investigate the role of nanofluid fouling on thermal performance of a thermosiphon, and pointed out that the form of the deposited layer can be affected by nanofluid concentration, applied heat load, inclination of thermosiphon and operation time. Their experimental data clearly indicate that the existence of the deposited layer increases the thermal resistance, deteriorating heat transfer performance. Naturally, more power loss is expected since the deposited layer blocks the transport path of nanofluid.

Acknowledgments: This work has been generously supported by JSPS Grants-in-Aid for Scientific Research B, Grant Number 26740049 and Grant Number 26289046.

Author Contributions: Wenhao Zhang conducted the convective flow analysis on a nanofluid saturated metal foam under the guidance of Akira Nakayama, while Wenhao Li and Chen Yang carried out a series of clear fluid flow and heat transfer analyses under the guidance of Akira Nakayama, which eventually lead Wenhao Zhang to the analysis on a nanofluid saturated metal foam.

Conflicts of Interest: The authors declare no conflict of interest.

Abbreviations

List of Symbols

A	surface area (m^2)
a_f	specific surface ($1/\text{m}$)
A_{int}	interfacial area between the fluid and solid (m^2)
c	specific heat of nanofluid (J/kgK)
c_p	specific heat of nanoparticle (J/kgK)
c_s	specific heat of solid phase (J/kgK)
Da	Darcy number (-)
D_B	Brownian diffusion coefficient (m^2/s)
D_T	thermophoretic diffusion coefficient (m^2/s)
d_m	mean pore diameter (m)
d_p	nanoparticle diameter (m)
f, F, g, G	profile functions (-)
Hg	Hagen number (-)
h	wall heat transfer coefficient ($\text{W}/\text{m}^2\text{K}$)
h_v	volumetric heat transfer coefficient ($\text{W}/\text{m}^3\text{K}$)

H	channel height (m)
k	thermal conductivity of nanofluid (W/mK)
k_{BO}	Boltzmann constant (J/K)
k_{dis}	dispersion thermal conductivity (W/mK)
k_{stag}	stagnant thermal conductivity (W/mK)
K	permeability (m ²)
Nu_v	Interstitial Nusselt number (-)
Le	Lewis number (-)
n_j	unit vector pointing outward from fluid side to solid side (-)
n_{BT}	microscopic Brownian and thermophoretic diffusivity ratio (-)
N_{BT}	macroscopic Brownian and thermophoretic diffusivity ratio (-)
$Nu_{H,R}$	Nusselt number (-)
Nu_v	Interstitial Nusselt number (-)
p	pressure (Pa)
Pe	Peclet number (-)
Pr	Prandtl number of nanofluid (-)
$P.P.$	dimensionless pumping power (-)
q_0	wall heat flux (W/m ²)
r	radial coordinate (m)
R	tube radius (m)
t	time (s)
T	absolute temperature (K)
u_i	velocity vector (m/s)
V	representative elementary volume (m ³)
x_i	Cartesian coordinates (m)
x, y, z	Cartesian coordinates (m)
γ	parameter associated with temperature ratio (-)
ε	porosity (-)
ε^*	effective porosity (-)
ζ_k	transverse thermal dispersion coefficient (-)
$\eta(\zeta = 1 - \eta)$	dimensionless radial coordinate (-)
μ	viscosity (Pa·s)
ν	kinematic viscosity of nanofluid (m ² /s)
ρ	density of nanofluid (kg/m ³)
ϕ	nanoparticle volume fraction (-)

Special Symbols

$\tilde{\varphi}$	deviation from intrinsic average
$\overline{\varphi}$	average over the cross-section
φ^*	dimensionless variable
$\langle \varphi \rangle$	Daricican average
$\langle \varphi \rangle^{f,s}$	intrinsic average

Subscripts and Superscripts

B	bulk mean
bf	base fluid
dis	dispersion
f	fluid phase
p	nanoparticle
s	solid phase
w	wall

References

1. Dukhan, N. *Metal Foams: Fundamentals and Applications*; DEStech Publications, Inc.: Lancaster, PA, USA, 2013.
2. Calmidi, V.V.; Mahajan, R.L. The effective thermal conductivity of high porosity fibrous metal foams. *ASME Trans. J. Heat Transf.* **1999**, *121*, 466–471. [[CrossRef](#)]
3. Calmidi, V.V.; Mahajan, R.L. Forced convection in high porosity metal foams. *ASME Trans. J. Heat Transf.* **2000**, *122*, 557–565. [[CrossRef](#)]
4. Xuan, Y.; Roetzel, W. Conceptions for heat transfer correlations of nanofluids. *Int. J. Heat Mass Transf.* **2000**, *43*, 3701–3707. [[CrossRef](#)]
5. Lee, S.; Choi, S.U.S. Application of metallic nanoparticle suspensions in advanced cooling systems. *Int. Mech. Eng. Congress Exhib.* **1996**, *1996*, 1–12.
6. Lee, S.; Choi, S.U.S.; Li, S.; Eastman, J.A. Measuring thermal conductivity of fluids containing oxide nanoparticles. *J. Heat Transf.* **1999**, *121*, 280–289. [[CrossRef](#)]
7. Heris, S.Z.; Esfahany, M.N.; Etemad, S.G. Experimental investigation of convective heat transfer of Al₂O₃/water nanofluid in a circular tube. *Int. J. Heat Fluid Flow* **2007**, *28*, 203–210. [[CrossRef](#)]
8. Pak, B.C.; Cho, Y. Hydrodynamic and heat transfer study of dispersed fluids with submicron metallic oxide particles. *Exp. Heat Transf.* **1998**, *11*, 151–170. [[CrossRef](#)]
9. Chien, R.; Chuang, J. Experimental microchannel heat sink performance studies using nanofluids. *Int. J. Thermal Sci.* **2007**, *46*, 57–66. [[CrossRef](#)]
10. Yang, C.; Li, W.; Nakayama, A. Convective heat transfer of nanofluids in a concentric annulus. *Int. J. Thermal Sci.* **2013**, *71*, 249–257. [[CrossRef](#)]
11. Sakai, F.; Li, W.; Nakayama, A. A rigorous derivation and its applications of volume averaged transport equations for heat transfer in nanofluid saturated metal foam. In Proceedings of the International Heat Transfer Conference, Kyoto, Japan, 10–15 August 2014.
12. Kuwahara, F.; Yang, C.; Ando, K.; Nakayama, A. Exact solutions for a thermal nonequilibrium model of fluid saturated porous media based on an effective porosity. *J. Heat Transf.* **2011**, *133*. [[CrossRef](#)]
13. Yang, C.; Ando, K.; Nakayama, A. A local thermal non-equilibrium analysis of fully developed forced convective flow in a tube filled with a porous medium. *Transp. Porous Media* **2011**, *89*, 237–249. [[CrossRef](#)]
14. Yang, C.; Nakayama, A. A synthesis of tortuosity and dispersion in effective thermal conductivity of porous media. *Int. J. Heat Mass Transf.* **2010**, *53*, 3222–3230. [[CrossRef](#)]
15. Yang, C.; Liu, W.; Nakayama, A. Forced convective heat transfer enhancement in a tube with its core partially filled with a porous medium. *Open Transp. Phenom. J.* **2009**, *1*, 1–6. [[CrossRef](#)]
16. Zhang, W.; Li, W.; Nakayama, A. An analytical consideration of steady-state forced convection within a nanofluid-saturated metal foam. *J. Fluid Mech.* **2015**, *769*, 590–620. [[CrossRef](#)]
17. Buongiorno, J. Convective transport in nanofluids. *J. Heat Transf.* **2006**, *128*, 240–250. [[CrossRef](#)]
18. Quintard, M.; Whitaker, S. One and two equation models for transient diffusion processes in two-phase systems. *Adv. Heat Transf.* **1993**, *23*, 369–465.
19. Quintard, M.; Whitaker, S. Local thermal equilibrium for transient heat conduction: Theory and comparison with numerical experiments. *Int. J. Heat Mass Transf.* **1995**, *38*, 2779–2796. [[CrossRef](#)]
20. Cheng, P. Heat transfer in geothermal systems. *Adv. Heat Transf.* **1978**, *14*, 1–105.
21. Nakayama, A. *PC-Aided Numerical Heat Transfer and Convective Flow*; CRC Press: Boca, Raton, 1995; pp. 103–115.
22. Nakayama, A.; Kuwahara, F.; Hayashi, T. Numerical modelling for three-dimensional heat and fluid flow through a bank of cylinders in yaw. *J. Fluid Mech.* **2004**, *498*, 139–159. [[CrossRef](#)]
23. Yang, C.; Li, W.; Sano, Y.; Mochizuki, M.; Nakayama, A. On the anomalous convective heat transfer enhancement in nanofluids: A theoretical answer to the nanofluids controversy. *J. Heat Transf.* **2013**, *135*, 054504. [[CrossRef](#)]
24. Maiga, S.B.; Palm, S.J.; Nguyen, C.T.; Roy, G.; Galanis, N. Heat transfer enhancement by using nanofluids in forced convection flows. *Int. J. Heat Fluid Flow* **2005**, *26*, 530–546. [[CrossRef](#)]
25. Li, W.; Nakayama, A. Temperature dependency of thermophysical properties in convective heat transfer enhancement in nanofluids. *J. Thermophys. Heat Transf.* **2015**, *29*, 504–512. [[CrossRef](#)]
26. Aladag, B.; Halelfadl, S.; Doner, N.; Maré, T.; Duret, S.; Estellé, P. Experimental Investigations of the Viscosity of Nanofluids at Low Temperatures. *Appl. Energy* **2012**, *97*, 876–880. [[CrossRef](#)]

27. Corcione, M. Empirical Correlating Equations for Predicting the Effective Thermal Conductivity and Dynamic Viscosity of Nanofluids. *Energy Convers. Manag.* **2011**, *52*, 789–793. [[CrossRef](#)]
28. Bianco, V.; Chiacchio, F.; Manca, O.; Nardini, S. Numerical investigation of nanofluids forced convection in circular tubes. *Appl. Thermal Eng.* **2009**, *29*, 3632–3642. [[CrossRef](#)]
29. Kleinstreuer, C.; Feng, Y. Experimental and theoretical studies of nanofluid thermal conductivity enhancement: A review. *Nanoscale Res. Lett.* **2011**, *6*, 1–13. [[CrossRef](#)] [[PubMed](#)]
30. Liang, C.Y.; Yang, W.J. Modified single blow technique for performance evaluation on heat transfer surfaces. *Trans. ASME J. Heat Transf.* **1975**, *97*, 16–21. [[CrossRef](#)]
31. Nakayama, A.; Kuwahara, F.; Kodama, Y. An equation for thermal dispersion flux transport and its mathematical modelling for heat and fluid flow in a porous medium. *J. Fluid Mech.* **2006**, *563*, 81–96. [[CrossRef](#)]
32. Zhukauskas, A. Heat transfer from tubes in crossflow. *Adv. Heat Transf.* **1987**, *18*, 87–159.
33. Fried, J.J.; Combarous, M.A. Dispersion in porous media. *Adv. Hydrosci.* **1971**, *7*, 169–282.
34. Launder, B.E.; Spalding, D.B. The numerical computation of turbulent flow. *Comput. Meth. Appl. Mech. Eng.* **1974**, *3*, 269–289. [[CrossRef](#)]
35. Taylor, G.I. The Dispersion of matter in turbulent flow through a pipe. *Proc. R. Soc. A* **1954**, *223*, 446–468. [[CrossRef](#)]
36. Nakayama, A.; Ando, K.; Yang, C.; Sano, Y.; Kuwahara, F.; Liu, J. A study on interstitial heat transfer in consolidated and unconsolidated porous media. *Heat Mass Transf.* **2009**, *45*, 1365–1372. [[CrossRef](#)]
37. Taylor, G.I. Dispersion of soluble matter in solvent flowing slowly through a tube. *Proc. R. Soc. A* **1953**, *219*, 186–203. [[CrossRef](#)]
38. Gelhar, L.W.; Axness, C.L. Three-dimensional stochastic analysis of macrodispersion in aquifers. *Water Resour. Res.* **1983**, *19*, 161–180. [[CrossRef](#)]
39. Wang, J.; Kitanidis, P.K. Analysis of macrodispersion through volume averaging: Comparison with stochastic theory. *Stoch. Environ. Res. Risk Assess.* **1999**, *13*, 66–84. [[CrossRef](#)]
40. Ohsawa, S. Three-Dimensional Simulation of Heat and Fluid Flow in a Nanofluid Saturated Metal Foam. Mater's Thesis, Graduate School of Engineering, Shizuoka University, Shizuoka, Japan, 2015.
41. Sarafraz, M.M.; Hormozi, F.; Peyghambarzadeh, S.M. Role of nanofluid fouling on thermal performance of a thermosyphon: Are nanofluids reliable working fluid? *Appl. Thermal Eng.* **2015**, *82*, 212–224. [[CrossRef](#)]



© 2016 by the authors; licensee MDPI, Basel, Switzerland. This article is an open access article distributed under the terms and conditions of the Creative Commons by Attribution (CC-BY) license (<http://creativecommons.org/licenses/by/4.0/>).